JEM Journal of Experimental Medicine

ARTICLE

NF-κB subunits RelA and c-Rel selectively control CD4+ T cell function in multiple sclerosis and cancer

Guilhem Lalle[1*], Raphaëlle Lautraite[1*], Khaled Bouherrou[1], Maud Plaschka[1], Aurora Pignata[2], Allison Voisin[1], Julie Twardowski[1], Marlène Perrin-Niquet[1], Pierre Stéphan[1], Sarah Durget[1], Laurie Tonon[3], Maude Ardin[3], Cyril Degletagne[1], Alain Viari[3], Laurence Belgarbi Dutron[4], Nathalie Davoust[5], Thomas S. Postler[6], Jingyao Zhao[6], Christophe Caux[1], Julie Caramel[1], Stéphane Dalle[1], Philippe A. Cassier[1], Ulf Klein[7], Marc Schmidt-Supprian[8,9,10], Roland Liblau[2], Sankar Ghosh[6], and Yenkel Grinberg-Bleyer[1]

The outcome of cancer and autoimmunity is often dictated by the effector functions of CD4+ conventional T cells (Tconv). Although activation of the NF-κB signaling pathway has long been implicated in Tconv biology, the cell-autonomous roles of the separate NF-κB transcription-factor subunits are unknown. Here, we dissected the contributions of the canonical NF-κB subunits RelA and c-Rel to Tconv function. RelA, rather than c-Rel, regulated Tconv activation and cytokine production at steady-state and was required for polarization toward the TH17 lineage in vitro. Accordingly, RelA-deficient mice were fully protected against neuroinflammation in a model of multiple sclerosis due to defective transition to a pathogenic TH17 gene-expression program. Conversely, Tconv-restricted ablation of c-Rel impaired their function in the microenvironment of transplanted tumors, resulting in enhanced cancer burden. Moreover, Tconv required c-Rel for the response to PD-1-blockade therapy. Our data reveal distinct roles for canonical NF-κB subunits in different disease contexts, paving the way for subunit-targeted immunotherapies.

Introduction

Conventional CD4+Foxp3− T cells (Tconv) exhibit pleiotropic functions in immunity. While they are critical for the clearance of a broad spectrum of pathogens, a growing body of literature suggests that Tconv are also potent effectors of antitumor responses. Their accumulation and activation are frequently associated with good prognosis in solid cancers, and the response to cancer immunotherapies such as checkpoint blockade–based therapies seems to be correlated with proper Tconv function (Borst et al., 2018; Cohen et al., 2022). Conversely, uncontrolled Tconv activation promotes autoimmune manifestations; for instance, they are key players in Crohn's disease, rheumatoid arthritis, or multiple sclerosis (MS) (Christophersen et al., 2019). This spectrum of functions relies on a myriad of different Tconv subsets. Indeed, the type of antigenic stimulation and the cytokine microenvironment drive the polarization toward different flavors of T helper (TH) cells that display selective roles in immune responses (Zhu and Paul, 2010). For instance, TH1 and T follicular helper (TFH) cells were shown to orchestrate immune responses to tumors (Borst et al., 2018), whereas granulocyte macrophage-colony stimulating factor (GM-CSF)–producing pathogenic TH17 cells emerge as the main drivers of MS and its murine model experimental autoimmune encephalomyelitis (EAE) (Codarri et al., 2011; Croxford et al., 2015).

In addition to specific transcription factors that drive the effector functions of each TH subset, a series of pioneering transcriptional regulators has been proposed to impact the fate of naive Tconv. Downstream molecules, nuclear factor of activated T cells (NFAT), activator protein 1 (AP-1), or Forkhead box protein O, as well as nuclear factor kappa B (NF-κB) transcription factors are required for the activation, proliferation, and cytokine expression of Tconv (Shah et al., 2021). However,

[1]Cancer Research Center of Lyon, Labex DEV2CAN, Institut Convergence Plascan, Centre Léon Bérard, UMR INSERM 1052, CNRS 5286, Université Claude Bernard Lyon 1, Lyon, France; [2]Toulouse Institute for Infectious and Inflammatory Diseases (Infinity), UMR INSERM 1291, CNRS 5051, Université Toulouse III, Toulouse, France; [3]Cancer Research Center of Lyon, Labex DEV2CAN, Institut Convergence Plascan, Centre Léon Bérard, Gilles Thomas Bioinformatics Platform, UMR INSERM 1052, CNRS 5286, Université Claude Bernard Lyon 1, Lyon, France; [4]Biology Department, Ecole Normale Supérieure of Lyon, Lyon, France; [5]Laboratory of Biology and Modelling of the Cell, Ecole Normale Supérieure of Lyon, CNRS UMR 5239, INSERM U1293, Lyon, France; [6]Department of Microbiology and Immunology, College of Physicians and Surgeons, Columbia University, New York, NY, USA; [7]Division of Haematology and Immunology, Leeds Institute of Medical Research at St. James's, University of Leeds, Leeds, UK; [8]Institute of Experimental Hematology, School of Medicine, Technical University of Munich, Munich, Germany; [9]Center for Translational Cancer Research, School of Medicine, Technical University of Munich, Munich, Germany; [10]German Cancer Consortium and German Cancer Research Center, Heidelberg, Germany.

*G. Lalle and R. Lautraite contributed equally to this paper. Correspondence to Yenkel Grinberg-Bleyer: yenkel.grinberg-bleyer@inserm.fr.

whether these proteins selectively dictate the fate of Tconv and TH cells in different diseases is unknown.

NF-κB is composed of a series of five subunits that share a Rel-homology domain and modulate transcription as homo- or heterodimers. NF-κB proteins are classically split into two families: NF-κB1, RelA (encoded by *Rela*), and c-Rel (*Rel*) belong to the canonical pathway, whereas NF-κB2 and RelB are alternative subunits (Oeckinghaus et al., 2011). The involvement of NF-κB in T cell biology has long been known through the use of mouse models carrying germline or conditional ablation of upstream regulators of the NF-κB pathway (reviewed in Gerondakis et al., 2014; Voisin and Grinberg-Bleyer, 2021). NF-κB is constitutively activated in tissues exposed to chronic inflammation, such as the brain of patients with MS, and may even serve as a biomarker for relapse (Mc Guire et al., 2013; Satoh et al., 2008; Yan et al., 2018). In line with this, T cell–restricted ablation of the upstream kinase *IKK2* confers resistance to EAE in mice (Greve et al., 2007). Conversely, impaired activation of NF-κB has been shown in T cells from patients with cancer (Li et al., 1994); moreover, in mice, anergic T cells, which resemble tumor-infiltrating exhausted cells, display decreased NF-κB activity (Clavijo and Frauwirth, 2012). Consistent with this idea, constitutive NF-κB activation in T cells has been shown to drive tumor rejection in mouse models (Barnes et al., 2015b). Furthermore, the efficacy of checkpoint blockade therapies relies on CD28 signaling in T cells, a cascade that triggers NF-κB activation (Kamphorst et al., 2017). RNA sequencing (RNA-seq) analyses highlighted the enrichment of NF-κB–driven signatures in patients responding to anti-programmed cell death 1 (PD-1) and anti-CTLA-4 therapies (Grasso et al., 2021).

Nevertheless, the selective contribution of each NF-κB subunit to the activation and differentiation processes of T cells in cancer and autoimmunity remains elusive. Such investigations have so far been prevented by the lack of adequate models: for instance, germline ablation of *Rela* leads to embryonic lethality (Beg et al., 1995), whereas *Relb* deficiency drives systemic autoimmunity (Weih et al., 1995). Data on the Tconv-autonomous roles of alternative NF-κB subunits are scarce (Lalle et al., 2021a), though canonical signaling seems to play the most critical role in Tconv biology. The use of *Rel*-deficient animals, as well as the recent identification of *REL*-mutant patients, has highlighted the role of this subunit in Tconv proliferation, IL-2 expression, as well as TH17 differentiation, although this latter parameter remains controversial, the same being true for RelA (Beaussant-Cohen et al., 2019; Hilliard et al., 2002; Lévy et al., 2021; Powolny-Budnicka et al., 2011; Ruan et al., 2011; Visekruna et al., 2010). *Rel*- and *Nfkb1*-deficient mice are largely resistant to EAE (Chen et al., 2011; Hilliard et al., 2002). Reciprocally, canonical NF-κB activation in all T cells is required to control cancer growth, though this phenotype likely relies on CD8$^+$ T cell–intrinsic mechanisms (Barnes et al., 2015a). It remains unclear whether the two closely related proteins RelA and c-Rel exhibit distinct contributions to the development and function of T cell subsets. Our recent studies suggested a context-dependent role for these transcription factors in Foxp3$^+$ regulatory T cells (Tregs) (Grinberg-Bleyer et al., 2017, 2018; Oh et al., 2017), but their putative roles in Tconv are understudied. Here, we used a series of conditional knock-out (cKO) mouse models and gene-edited primary human cells to bridge the knowledge gap on the functions of RelA and c-Rel in Tconv at steady-state in EAE and cancer.

Results

NF-κB RelA directs Tconv activation at steady-state

We first aimed at deciphering the distinct roles of RelA and c-Rel in regulating Tconv biology at steady-state. *CD4*^{cre} mice were crossed with animals carrying floxed alleles for *Rela* or *Rel* (hereafter named cKO for conditional knock-out mice), resulting in the ablation of these genes in all T cell subsets accompanied by green fluorescent protein (GFP) expression (Heise et al., 2014). Of note, the relative distribution and cell numbers of T cell subsets in the thymus were maintained in the absence of either RelA or c-Rel, with the exception of impaired Treg cell development in *Rel*-cKO mice, as we and others previously reported (Oh et al., 2017; Webb et al., 2019) (Fig. S1, A–D and F). Nevertheless, we detected a slight but significant reduction in the number of Tconv and CD8$^+$ T cells in the lymph nodes (LN) and spleens of *Rela*-cKO mice (Fig. S1, A–E). To examine Tconv cell intrinsic functions of NF-κB subunits, we performed mixed bone marrow (BM) transfer experiments of CD45.1$^+$ cells and control or cKO CD45.2$^+$ cells (Fig. 1 A). Flow cytometric analysis of spleen cells 8 wk after BM transfer revealed a competitive disadvantage of *Rela*, but not *Rel*, -deficient T cells (Fig. 1 B). The accumulation of Tregs was strongly impaired in the absence of either RelA or c-Rel (Fig. S1 G). Among CD4$^+$Foxp3$^-$ Tconv, we detected a reduction of activated CD44^{high} (in particular CD44^{high}CD62L^{low} effector memory cells) and proliferating Ki67$^+$ cells in the *Rela*-cKO compartment and to a lesser extent in the *Rel*-cKO BM compared with controls (Fig. 1 C and Fig. S1 H). Next, we examined cytokine expression following polyclonal restimulation. We found that RelA played a more prominent role than c-Rel in the expression of classical T cell cytokines IL-2 and IFNγ; in contrast, the proportion of TNF-α$^+$ cells was not significantly impacted in the absence of NF-κB, although a trend could be detected (Fig. 1 D).

To gain insight into the regulation of gene expression by NF-κB subunits, we then conducted RNA-seq analyses on control and mutant Tconv, stimulated with anti-CD3/CD28 and IL-2 for 4 h. Differential gene expression analyses revealed large alterations in the transcriptome of *Rela*-cKO Tconv, with 933 genes being significantly up- or downregulated. In comparison, *Rel*-cKO Tconv displayed a lower level of transcriptomic modifications, with 199 differentially expressed genes (DEGs), among which only 16 were specific to *Rel*-cKO cells (Fig. 1, E and F; and Fig. S1 I). Among the genes altered in *Rela*-cKO Tconv, many were activation markers (such as *Cd83*, *Icos*, and *Tnfrsf9*), as well as inducible cytokines (notably the TH1/2/17 cytokines *Ifng*, *Il4*, and *Il17a*) and chemokines (Fig. 1 G). *Tnf* expression appeared decreased in *Rela* and *Rel*-cKO transcriptomes. This discrepancy with FACS data may be owing to posttranscriptional regulation (Stamou and Kontoyiannis, 2010) or to the FACS experimental scheme, which implies strong restimulation with PMA and ionomycin. Interestingly, a series of IFN-signaling and IFN-

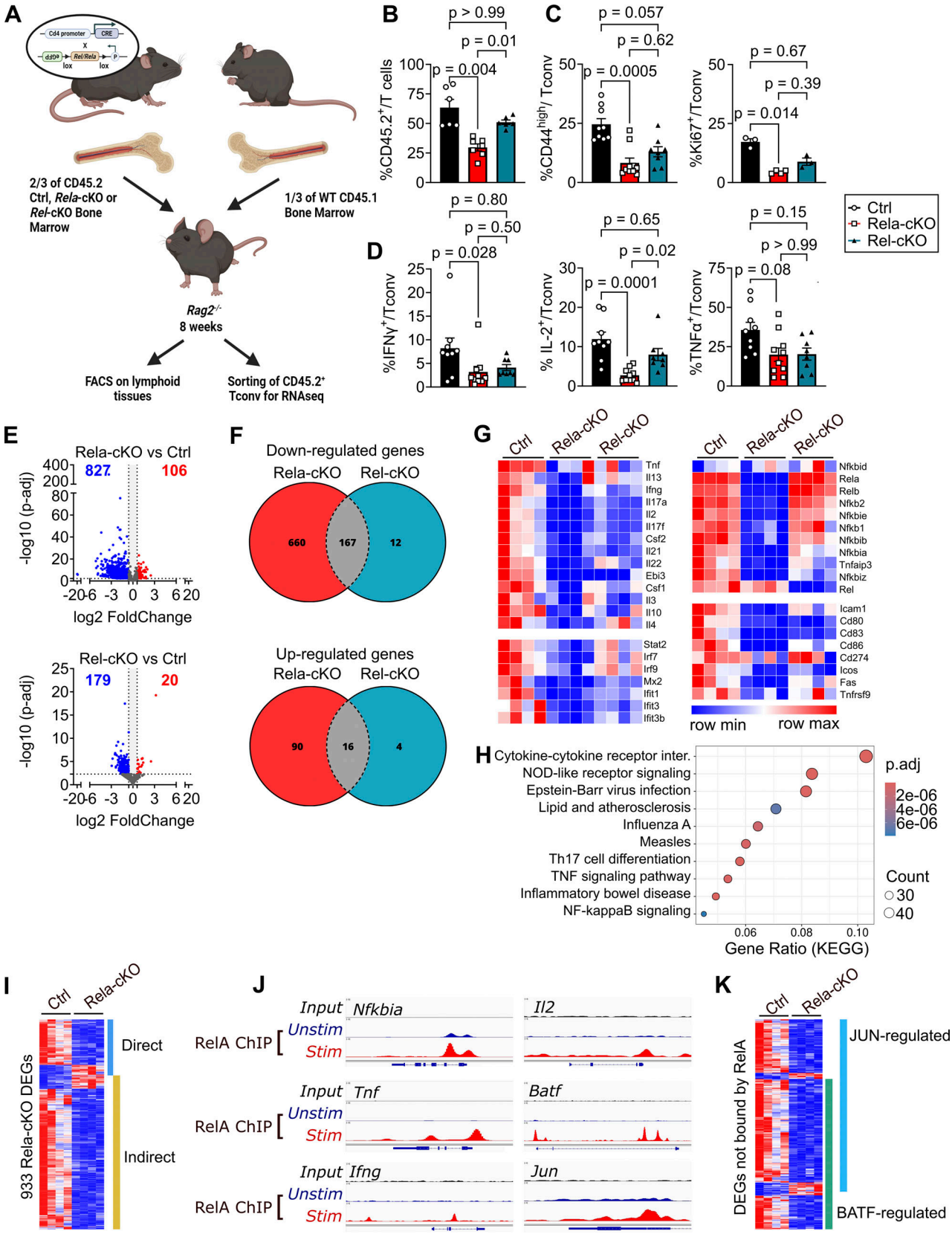

Figure 1. **Mouse Tconv homeostasis and transcriptome are predominantly controlled by NF-κB RelA. (A)** Schematic representation of the experimental mixed BM chimera model used (control = $CD4^{cre}$). **(B–D)** Spleen cells were analyzed by flow cytometry (mean ± SEM of n = 3–10 mice/group from two experiments). **(B)** Proportion of T cells that are of CD45.2 origin. **(C)** Proportion of $CD44^{high}$ and $Ki67^{+}$ in $CD45.2^{+}TCR\beta^{+}CD4^{+}CD8^{-}Foxp3^{-}$ Tconv. **(D)** Spleen cells were restimulated with PMA-ionomycin; proportions of cytokine expression by $CD45.2^{+}$ Tconv are shown. **(E–H)** RNA-seq analysis of $CD45.2^{+}$ Tconv

sorted from spleen and LN and stimulated for 4 h with anti-CD3/CD28 and IL-2 (n = 4 independent samples/genotype [two mice/sample] from two experiments sequenced simultaneously). **(E)** Volcano plot of DEGs (log_2 fold change >0.58, P < 0.005). Bold numbers denote the numbers of downregulated (blue) and upregulated (red) genes. **(F)** Venn partition diagram showing the overlap between RelA and c-Rel–regulated DEGs. **(G)** Heatmaps of selected DEGs. **(H)** KEGG enrichment analysis of *Rela*-cKO DEGs. **(I and J)** RelA DNA-binding analysis in WT Tconv (Oh et al., 2017) stimulated or not with anti-CD3/CD28 for 4 h. **(I)** Heatmap of DEGs directly (in blue) and indirectly (in yellow) bound by RelA. **(J)** Visualization of RelA binding in selected loci using Integrative Genome Viewer. **(K)** BATF and c-Jun binding on DEGs not directly bound by RelA. Our RNA-seq and ChIP-Seq data were compared to publicly available ChIP-Seq data of BATF and c-Jun. The heatmap represents DEG in *Rela*-cKO cells that might be regulated by these proteins. For FACS data, Kruskal–Wallis tests were used.

stimulated genes were also downregulated (e.g., *Mx2*, *Ifit1*, and *Irf7*). As shown in other cell types, RelA was also necessary for the optimal expression of NF-κB pathway–related genes (e.g., *Tnfaip3*, *Nfkbia*, and even other NF-κB subunits). Gene ontology analyses highlighted altered cytokine/cytokine receptor interactions as well as various inflammation-related signatures and NF-κB signaling as expected upon *Rela*-ablation (Fig. 1 H and Fig. S1 J). Thus, RelA rather than c-Rel seems to be a prime determinant of Tconv activation ex vivo. To gain further insight into the regulation of gene expression by RelA, we used our previously published RelA chromatin immunoprecipitation followed by deep sequencing (ChIP-Seq) data from CD3/CD28 stimulated Tconv (Oh et al., 2017) (GSE99319). Intriguingly, out of the 933 DEGs in *Rela*-cKO Tconv, only 249 were directly bound by RelA (Fig. 1 I), including expected targets such as *Nfkbia*, *Tnf*, or *Ifng*, but also a series of 34 transcription regulators (transcription factors or epigenetic regulators) including the AP-1 members Jun and BATF (Fig. 1 J and Fig. S1, K and L). Interestingly, by using public ChIP-Seq databases in T cells (Liu et al., 2019), we found that BATF and c-Jun were bound to nearly all 684 genes indirectly regulated by RelA (Fig. 1 K). These transcription factors were largely involved in T cell activation and function, including in cancer (Betz et al., 2010; Seo et al., 2021). These observations thus provide a mechanistic understanding of gene regulation by NF-κB in Tconv and highlight a crosstalk between NF-κB and MAPK pathways.

The contribution of RelA and c-Rel to human Tconv identity

Despite the recent description of few patients carrying loss-of-function *RELA* or *REL* mutations (Badran et al., 2017; Beaussant-Cohen et al., 2019; Comrie et al., 2018; Lévy et al., 2021; Moriya et al., 2023), T cell–autonomous functions of these subunits in humans are unclear. We developed a CRISPR-Cas9/ribonucleoprotein (RNP) electroporation approach to ablate *RELA* or *REL* in in vitro stimulated primary human Tconv from healthy donors (Fig. 2 A). This approach regularly led to over 90% RELA and C-REL deletion at the protein level (Fig. 2 B). We first deciphered gene expression patterns in control and mutant cells by RNA-seq after 4 h of restimulation with anti-CD3/CD28 and IL-2. Whereas only 12 genes were altered in *REL*-deficient cells, loss of *RELA* caused significant changes in the expression of 378 genes (of those, six were common to $REL^{-/-}$ cells) (Fig. 2 C and Fig. S2 A). As for mouse cells, human RELA controlled the expression of genes related to NF-κB and other signaling pathways, activation markers, as well as cytokines and chemokines (Fig. 2 D). This was further confirmed by gene enrichment analyses, which reinforced the likely involvement of *RELA* in TH17 cells (Fig. S2 B). Of note, out of the 172 downregulated human genes in $RELA^{-/-}$ that had mouse orthologs, 80 were also found significantly downregulated in our mouse data; the correlation was weaker for upregulated genes (Fig. S2 C). This relatively poor correlation between mouse and human transcriptomes was likely due to the fact that NF-κB ablation in human cells was conducted after a first round of stimulation, thus hindering the possible roles of RELA and c-REL in the early transcriptional program of Tconv. Nevertheless, Kyoto Encyclopedia of Genes and Genomes (KEGG) enrichment analyses on common downregulated genes highlighted once again the involvement of RELA in TH17 signature genes (Fig. S2 D). Next, we explored the proliferative capacity of Tconv in vitro and found that *REL* ablation, but not *RELA*, significantly altered Tconv cell cycle after 4 days of culture with anti-CD3/28 stimulation. In line with previous reports, this defect was rescued by exogenous IL-2 (Fig. 2, E–G) (Beaussant-Cohen et al., 2019; Lévy et al., 2021). In addition, FACS analyses following PMA-ionomycin restimulation showed a reduction of both TNF-α– and IL-2–expressing $RELA^{-/-}$ cells compared with the control, whereas *REL* deletion only impaired TNF-α expression (Fig. 2, F and G). In contrast to RNA-seq data, IFNγ expression was not significantly changed in the absence of *RELA* or *REL*; this could be due to either strong variability between donors, possible posttranscriptional regulation as previously described (Pesu et al., 2006; Sareneva et al., 1993), or the PMA-ionomycin restimulation protocol used for FACS analyses. In summary, these results reinforce the role of RelA in shaping the transcriptome of Tconv both in mice and humans.

Selective functions of RelA and c-Rel in TH cell polarization

Because our transcriptome analyses suggested cell-autonomous roles for NF-κB subunits in TH differentiation, we next performed in vitro culture assays using naive Tconv from control and cKO mice. We first measured whether canonical NF-κB was involved in the proliferation of naive cells and found a trend toward reduced proliferation in the absence of *Rel*, which was surprisingly more pronounced in the presence of exogenous IL-2 (Fig. S3 A and Fig. 3 A). To verify whether the level of stimulation may influence the phenotype of NF-κB–deficient cells, we also tested their proliferation following culture with suboptimal doses of anti-CD3 and feeders (1:4 and 1:10 of the maximum dose). Surprisingly, c-Rel ablation did not impact Tconv cell division in these settings (Fig. S3 B), suggesting that the role of c-Rel in Tconv proliferation was restricted to a precise range of engagement of the TCR and costimulatory receptors. In TH1-polarizing conditions and with maximal anti-CD3/feeder concentrations, the proportion of $IFN\gamma^+$ cells was significantly altered in the absence of RelA, but not c-Rel (Fig. 3 B), without affecting the expression of the TH1 master transcription factor T-Bet. Consistent with published data (Balasubramani et al.,

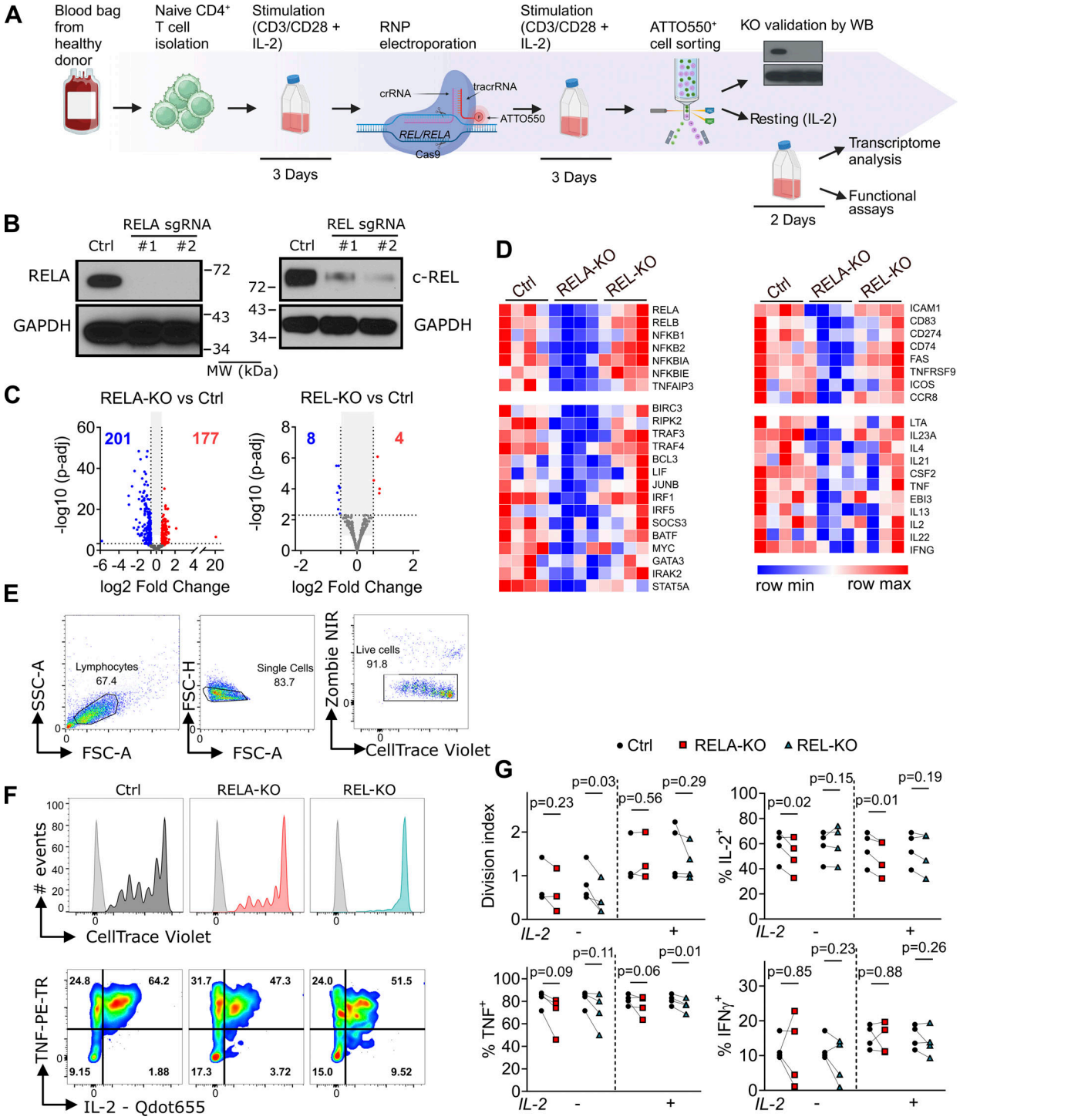

Figure 2. **Separate roles of RELA and c-REL in human Tconv. (A)** Experimental protocol; created with https://Biorender.com. **(B)** Western blot validation of gene editing efficacy after ATTO550+ live cell sorting (one representative of four experiments). **(C and D)** RNA-seq analysis following a 4 h stimulation with anti-CD3/CD28 and IL-2 (n = 4 experiments with one donor/experiment, sequenced simultaneously). **(C)** Volcano plot of DEGs (log_2 fold change >0.58, P < 0.005). Bold numbers denote the number of downregulated (blue) and upregulated (red) genes. **(D)** Heatmaps of selected DEGs. **(E–G)** Gene-edited Tconv were sorted and rested for 2 days and then labeled with Cell Trace Violet (CTV) and stimulated 3 days with anti-CD3/CD28 and IL-2. Cells were analyzed by FACS after PMA-ionomycin restimulation. **(E)** Gating strategy for Tconv cell analysis. **(F)** Representative CTV (top, gray histograms denote unstained controls) and cytokine (bottom) staining (one representative of three experiments). **(G)** Cumulative data from n = 3–4 experiments with independent donors. Multiple paired T tests were used. Source data are available for this figure: SourceData F2.

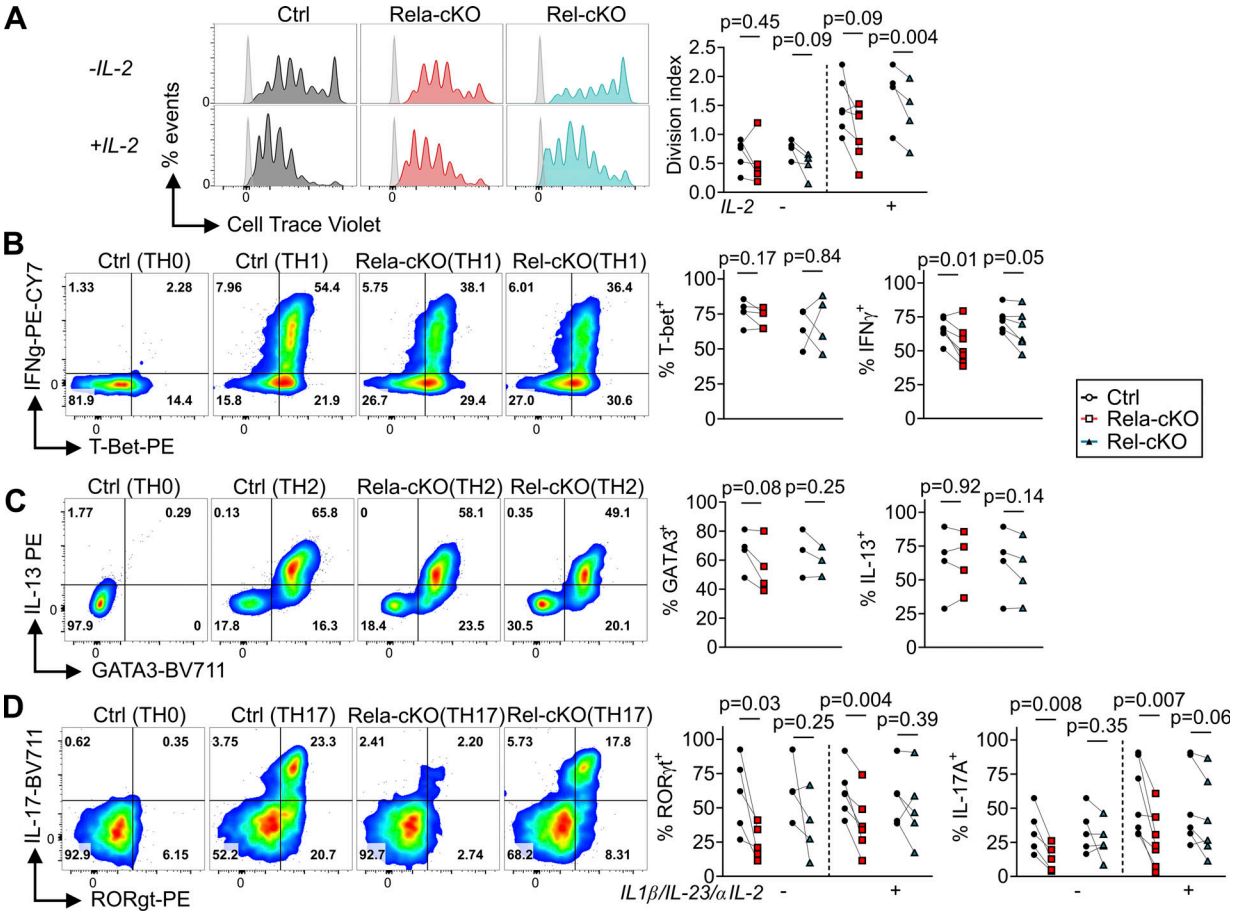

Figure 3. **The roles of RelA and c-Rel in TH polarization in vitro. (A–E)** Naive Tconv from control (CD4^{cre}), *Rela*-cKO, and *Rel*-cKO mice were isolated, stimulated with high concentration of soluble anti-CD3 and feeders, and cultured with or without IL-2 (A), or under Th1 (B), Th2 (C), or Th17 (D) for 4 days as detailed in Materials and methods, and their phenotype was analyzed by FACS after PMA-ionomycin restimulation. Representative (left panels) and cumulative (right) data from at least three experiments are shown. Each line represents an independent experiment; multiple paired *t* tests were used.

2010), RelA was bound to the *Ifng* locus in anti-CD3/CD28 stimulated cells but also to T-Bet (Fig. 1 J and Fig. S3 F). Again, this role of NF-κB was lost upon stimulation with lower amounts of stimulation (Fig. S3 C). In TH2 differentiation, GATA-3 expression was slightly decreased, though not significantly, exclusively in *Rela*-cKO cells (Fig. 3 C). This is in line with a recent report (Henriksson et al., 2019) and was associated with direct RelA binding to an intronic region of the *Gata3* locus (Fig. S3 F). IL-13 expression was not impacted by NF-κB ablation at any of the stimulation doses tested, while Il4, Il5, or Il13 loci were not bound by RelA (Fig. 3 C and Fig. S3, D and F). Finally, we detected a selective contribution of RelA in the differentiation of TH17 cells (Fig. 3 D). Indeed, the number of RORγt$^+$ and IL-17A$^+$ cells decreased by ∼50% in the absence of RelA in "classical" (TGF-β+IL-6) culture conditions, whereas *Rel*-deficient cells showed unaltered differentiation. This intriguing phenotype was further confirmed when inflammatory cytokines (IL1β+IL-23+anti-IL-2) were added to the culture. Stimulation with suboptimal doses of anti-CD3 and feeders confirmed the critical role of RelA but also revealed a decrease in IL-17A expression with Rel-deficient Tconv in the TGF-β+IL-6 condition (Fig. S3 E). This finding may explain why certain reports showed reduced TH17 differentiation in vitro (Ruan et al., 2011), while others did not (Powolny-Budnicka et al., 2011; Visekruna et al., 2010). Mechanistically, RelA bound directly to the *Rorc* locus, even in "TH0" conditions, but not to the *Il17a* locus (Fig. S3 F). To understand whether this general impairment of *Rela*-deficient cells resulted from a role in the initial priming of naive Tconv rather than a function in TH-lineage specification, we also analyzed the expression of CD44 after 24 h of stimulation, but no difference could be detected between control and *Rela*-deficient Tconv (Fig. S3 G). These data thus illustrate major contributions of RelA to in vitro TH subset differentiation.

RelA promotes Tconv pathogenicity in EAE

Next, we investigated the in vivo relevance of these findings in the context of autoimmunity. We used an active EAE model, relying on the activity of GM-CSF–producing Tconv that adopt a pathogenic TH17 phenotype (TH17p cells). Whereas control mice developed a severe EAE, we observed drastic protection of *Rela*-cKO mice against disease development. Indeed, only ∼20% of the animals developed detectable clinical symptoms, and their maximal scores peaked at 1.5 (Fig. 4, A–C). This protection was substantiated at the histological level. Luxol Fast Blue staining of

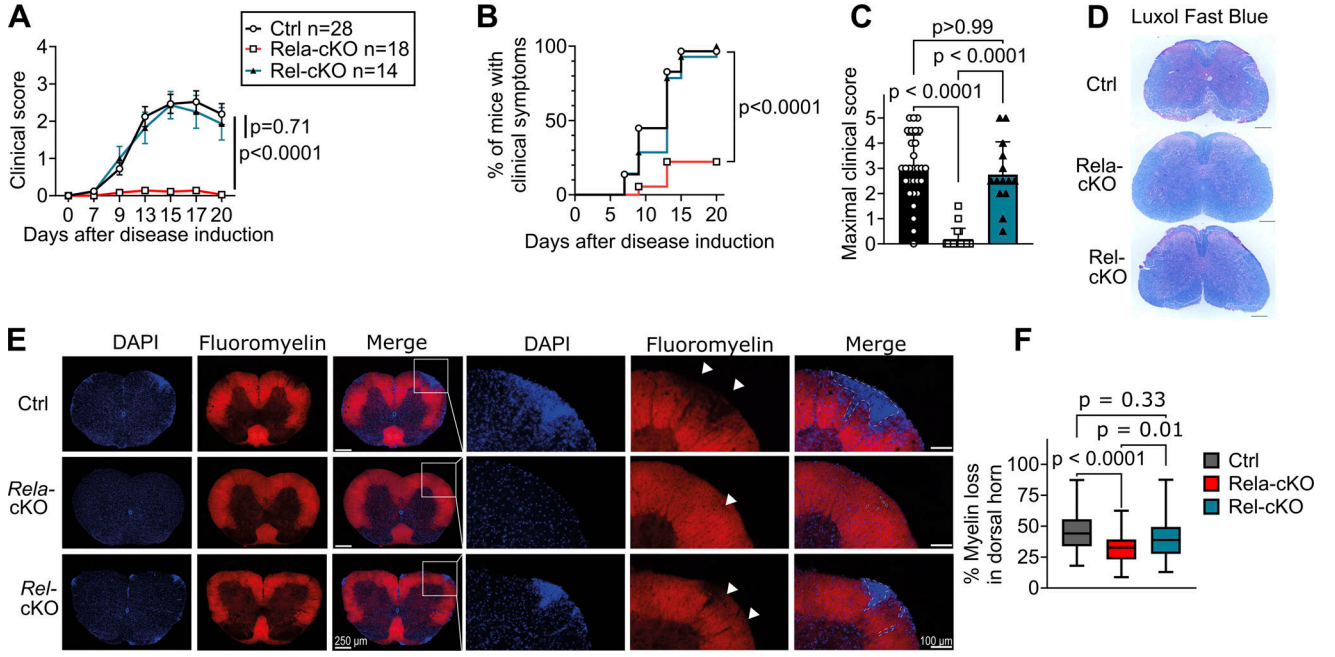

Figure 4. **T cell–restricted ablation of RelA, but not c-Rel, protects against EAE.** EAE was induced in control (CD4^{cre}), *Rela*-cKO, and *Rel*-cKO mice in a specific and opportunistic pathogen–free animal facility (CRCL, Lyon, France). **(A)** Disease score curves (n = 14–28 mice/group from five independent experiments). **(B)** Disease incidence. **(C)** Maximal clinical score. **(D)** Sections of spinal cords at D15 were stained with Luxol Fast Blue; representative images from four to five mice/genotypes of two independent experiments are shown. The dotted line underlines the border between demyelinated area of the tissue and normal white matter (homogenous blue staining). Most of the time, the demyelinated area juxtaposed immune cells infiltration revealed by the counterstaining with nuclear red. Scale bars = 200 µm. **(E and F)** Sections of spinal cords at D15 were stained for Fluoromyelin and DAPI. Representative images (E) and proportion of myelin loss in the dorsal horn from 35 to 59 cross-sections, from four to five mice/genotype of two independent experiments (F) are shown; scale bars = 250 µm (left) and 100 µm (right). Arrowheads point to demyelinated areas of the dorsal horn. In A, C, and E, mean ± SEM are shown. Two-way ANOVA followed by Bonferroni's post-test (A), Log-rank (Mantel–Cox) (B), and Kruskal–Wallis tests (C and F) were used.

spinal cords at day 15 (D15) revealed demyelinated areas in the white matter of control and *Rel*-cKO, but not *Rela*-cKO, tissues (Fig. 4 D). Specifically, fluoromyelin immunofluorescence highlighted decreased destruction of myelinated areas in the dorsal horn of the spinal cord (Fig. 4, E and F; and Fig. S3 H). In addition, whereas active EAE in control mice led to massive activation of microglia and other myeloid cells in the central nervous system (CNS), this process was abolished in the absence of RelA, as assessed by MHC-II and Iba1 expression by FACS and immunofluorescence, respectively (Fig. S3, I–M). In contrast, *Rel* deficiency in T cells did not impact the onset or progression of EAE. Thus, RelA in Tconv has a critical and non-redundant function in promoting neuroinflammation. Accordingly, the total number of CNS-infiltrating Tconv was dramatically decreased in *Rela*-cKO but not *Rel*-cKO tissues, suggesting defective recruitment, proliferation, and/or survival in non-lymphoid tissues; these numbers were not altered in draining LNs (dLN) (Fig. 5 A).

To understand how RelA and c-Rel differentially shape Tconv function in EAE, we analyzed their transcriptome at the single-cell level by droplet-based single-cell RNA-seq (scRNA-seq) (10X Genomics). A total of 9,912 CD4$^+$ T cells from dLN and the CNS (pooled brain and spinal cord) of control, *Rela*-cKO, and *Rel*-cKO mice, 15 days after EAE induction, were successfully sequenced. As expected, Treg cell clusters could be detected in each tissue that were excluded from further analyses to specifically dissect Tconv identity (Fig. S4, A and B). In dLN, Seurat clustering led to the identification of five clusters (Fig. S4 C). We used top markers and known genes to annotate these populations (Fig. S4 D). Naive cells were characterized by high *Lef1*, *Ccr7*, *Sell*, and low *Cd44* expression and represented the majority of cells. In addition, we found a cluster of naive cells expressing high levels of IFN-stimulated genes (such as *Ifit1*, *Ifit3b*, *Isg15*...). An "intermediate" state was defined by the low expression of *Cd44* but high *Tnf* and *Nfkbid*. Finally, effector memory T cells (TEM) (*Sell*^{low} *Cd44*^{high}) and cycling (*Mki67*$^+$) cells were identified. The general distribution of these clusters was not different between genotypes, except for the IFN_signature cluster that was enriched in *Rela*-cKO dLNs (Fig. S4 E). DEG analysis showed that only 27 and 32 genes were statistically altered in *Rela* and *Rel*-cKO cells, respectively (Fig. S4 F). Thus, the ablation of single NF-κB subunits did not drive sizeable perturbations in Tconv distribution, activation, and transcriptome in LNs at this time point. In contrast, in the CNS, NF-κB ablation led to dramatic shifts in cell distribution. Overall, eight clusters could be identified, including naive-like and IFN_signature cells similar to those in dLN, but also TH1 cells (*Fasl*$^+$*Ifng*$^+$*Rorc*$^-$), classical TH17 (*Rorc*$^+$*Il17re*$^+$*Csf2*$^-$), as well as pathogenic TH17 (*Rorc*$^+$*Ifng*$^+$*Csf2*$^+$*Lta*$^+$) populations, and also two clusters of proliferating cells (Fig. 5, B–D; and Fig. S4 G). Comparing the distribution of these clusters between genotypes, we found a strong enrichment in naive-like cells in *Rela*-cKO mice at the expense of

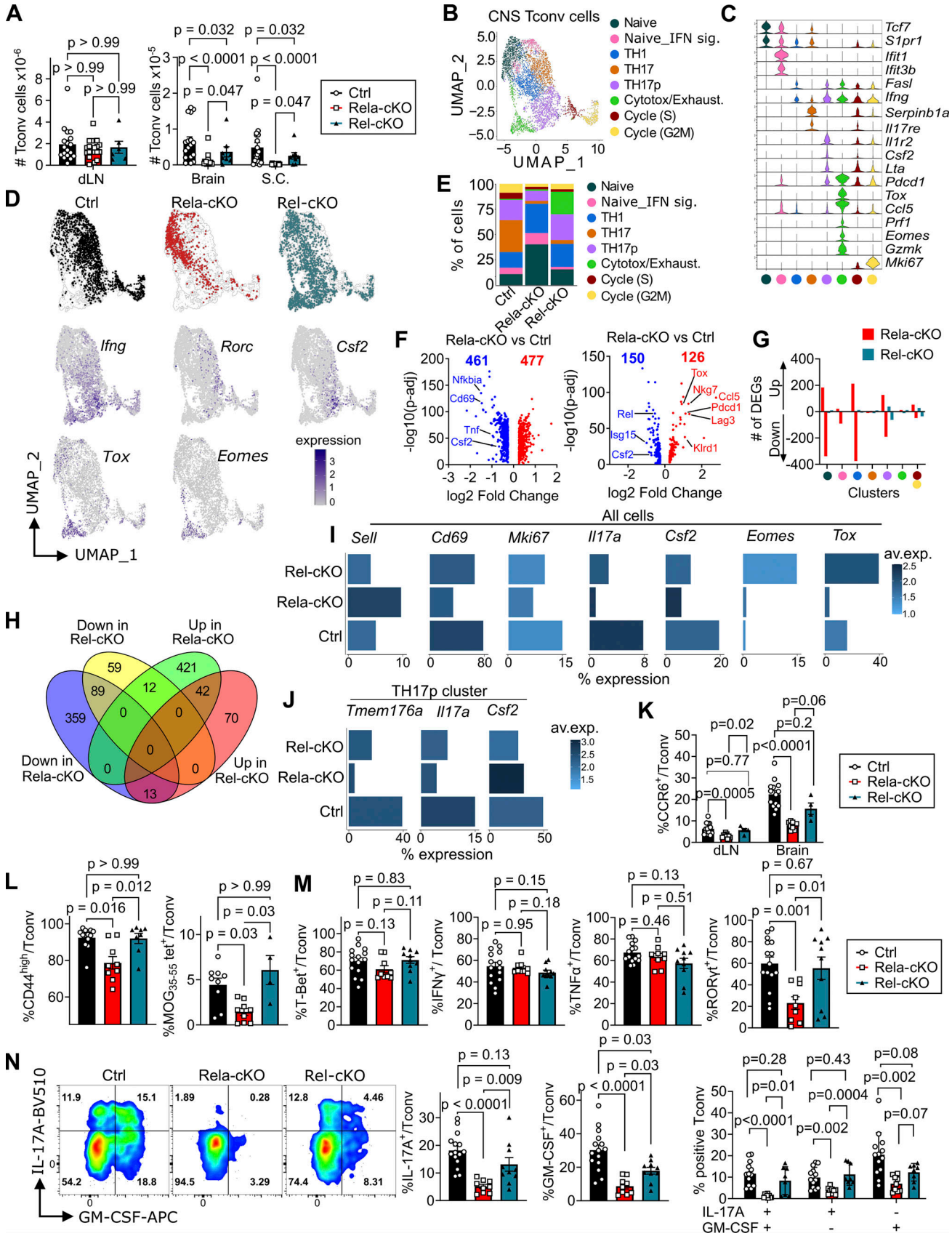

Figure 5. **RelA is required for Tconv pathogenic function in EAE.** EAE was induced in control (CD4^{cre}), *Rela*-cKO, and *Rel*-cKO mice in a specific and opportunistic pathogen–free animal facility (CRCL, Lyon, France). **(A)** Enumeration of CD45$^+$TCR-β$^+$CD4$^+$Foxp3$^-$CD8$^-$ cells at D15 in dLN, brain, and spinal cord (S.C.) (mean ± SEM of 6–18 mice/group from three independent experiments). **(B–J)** CD4$^+$ T cells were sorted from the CNS at D15 and analyzed by scRNA-seq

(performed once with 5–6 pooled mice/genotype). **(B)** Uniform Manifold Approximation and Projection (UMAP) representation and identification of Seurat clusters. **(C)** Violin plot showing expression of selected cluster-defining genes. **(D)** Cell distribution between genotypes (top) and expression of selected markers projected on UMAP (bottom). **(E)** Distribution of the eight clusters in each genotype. **(F)** Volcano plot representation of DEGs (blue: downregulated, red: upregulated, P-adj cutoff <0.05). **(G)** Number of DEGs in each cluster. **(H)** Venn diagram showing overlap of DEGs. **(I and J)** Percentage and intensity of expression of selected genes in all Tconv (I) and in the TH17p cluster specifically (J). **(K–N)** CNS-infiltrating Tconv were analyzed by FACS 20 days after disease induction, directly ex vivo (K and L) or after PMA-ionomycin restimulation (M and N) (data are representative of, or show the mean ± SEM of 4–15 mice/group from three independent experiments). Kruskal–Wallis tests were used.

TH17 and TH17p cell clusters (Fig. 5, D and E), supporting the critical role of RelA in TH17 polarization. Of note, although the proportion of TH17 cells was reduced in *Rel*-cKO mice, the TH17p cluster was maintained, possibly explaining the unaltered disease severity in these mice. In addition, a distinct cluster of cells harboring features of both exhaustion (*Tox*, *Lag3*, *Pdcd1*, *Havcr2*, and *Ccl5*) and cytotoxicity (*Eomes*, *Gzmk*, and *Klrd1*) with maintained expression of *Ifng* but devoid of *Rorc* or *Csf2* could be detected solely in *Rel*-cKO tissues and likely contributed to disease pathogenicity, as suggested in mice with EAE and patients with MS (Joulia et al., 2024; Raveney et al., 2015, 2021; Schafflick et al., 2020). The enrichment of "exhausted" and EOMES$^+$ cells in *Rel*-cKO CNS was substantiated at the protein level (Fig. S4 H). Overall, public TH17 signature scores were lower in the absence of RelA and to a lesser extent of c-Rel (Fig. S4 I). Importantly, the proportion of cells undergoing proliferation (S and G2M clusters) was reduced by about threefold in *Rela*-deficient and to a lesser extent in *Rel*-cKO Tconv (Fig. 5 E). This was corroborated by a reduction in total Ki67$^+$ cells and an impaired expression of cell cycle signature hallmarks (Fig. 5 I and Fig. S4 I). Hence, the ablation of RelA and c-Rel had distinct effects on the Tconv transcriptome. *Rela* deficiency had more pronounced effects, with over 900 DEGs; among those, 128 were shared with *Rel*-deficient cells, including *Cd69* or *Tnf*, but also TH17 hallmarks such as *Rorc*, *Tmem176a/b*, and even *Csf2* (Fig. 5, F–H). However, the impact of *Rela* ablation on the expression of these DEGs was more pronounced than that in *Rel*-deleted Tconv (Fig. 5 I). Of note, the number of DEGs in *Rela*-cKO tissues differed depending on the cell cluster, with strong changes in the naive, TH1, and TH17p subsets (Fig. 5 G). In the latter case, we detected a moderate decrease in *Rorc*-, *Il17a*-, *Csf2*-, and *Tmem176a*-expressing cells, suggesting that RelA was involved not only in the priming of the TH17 subset but also in the maintenance of its transcriptional program (Fig. 5 J).

In addition to an impaired proliferative capacity, the reduced Tconv accumulation in the CNS of Rela-deficient mice may also rely on perturbations in cell survival and/or migration toward the CNS. The proportion of Annexin V$^+$ apoptotic cells was unchanged in the absence of RelA, thereby infirming the first hypothesis (Fig. S4 J). In contrast, we detected a significant reduction in CCR6-expressing Tconv cells in Rela-cKO dLN and CNS, while only a trend could be observed in Rel-mutant animals (Fig. 5 K). As observed at the RNA level, the proportion of CD44^{high} effector/memory Tconv in dLN and their expression of cytokines was similar between strains (Fig. S4 K). In contrast, the proportion of CD44^{high} Tconv was reduced in the brain of *Rela*-cKO animals (Fig. 5 L). In line with this, MOG$_{33–55}$ tetramer staining demonstrated a defective accumulation of myelin oligodendrocyte glycoprotein (MOG)–specific T cells in the brain of *Rela*-cKO mice. TH1 hallmarks T-Bet, TNF-α, and IFNγ were identical in all strains (Fig. 5 M). In contrast, we detected major alterations in the expression of TH17-related cytokines and transcription factors RORγt, IL-17A, IL-17F, and GM-CSF in *Rela*-cKO Tconv (Fig. 5 N). The profile of *Rel*-cKO was largely similar to the controls, with the exception of decreased GM-CSF$^+$ cells independent of their IL-17 expression; this was in line with our scRNA-seq data and confirmed previous observations (Gerondakis et al., 1996). Thus, RelA activity in Tconv is critical for their pathogenicity in EAE by acting at different levels: (i) migration, (ii) in situ proliferation, and (iii) expression of inflammatory cytokines.

To investigate whether RelA may also be involved in the initial priming of Tconv prior to infiltration in the CNS and development of clinical signs, we examined the accumulation and activation status of MOG-specific Tconv in dLNs. Their proportion and antigen-experienced phenotype levels were not diminished in *Rela*-cKO mice compared with controls at D4 and D10, and even increased at D20 after immunization (Fig. 6 A). However, at D4, their expression of inflammatory cytokines IFNγ and GM-CSF was lower upon restimulation with MOG$_{33–55}$, suggesting a role for RelA in the early polarization of Tconv toward the TH17/TH17p lineage (Fig. 6 B). At D20, the proportion of IL17A$^+$ but not GM-CSF$^+$ cells, was increased in control dLN compared with D4. The level of each cytokine was still reduced in the absence of RelA, but to a lesser extent than at D4, likely due to the accumulation of MOG-specific T cells in the mutant dLN. To rule out a possible involvement of CD8$^+$ T cells, we also analyzed the incidence and severity of EAE in *Rela*-floxed mice crossed with the CD8a^{cre} (E8I^{cre}) background, thereby restricting the ablation of NF-κB to mature peripheral CD8$^+$ T cells. In this context, clinical scores were not reduced in *Rela*-mutant mice compared with controls, thereby confirming the role of RelA in CD4$^+$ cells (Fig. S4 L).

To better discriminate the putative functions of RelA in the priming and the maintenance of the disease, we crossed *Rela*-floxed mice with the CD4$^{cre\text{-}ERT2}$ strain (termed icKO for inducible cKO mice), enabling tamoxifen-inducible acute ablation of the gene in peripheral CD4$^+$ T cells. Interestingly, we observed that tamoxifen administration induced recombination, as evidenced by the expression of GFP, which was up to 10-fold higher in Tconv than that in Tregs and reached 60–80% of Tconv depending on the time point (Fig. S4, M and N). Thus, this strategy allowed to spare CD8$^+$ T cells and the vast majority of Tregs from *Rela* excision, enabling the Tconv cell–intrinsic study of RelA. When tamoxifen was administered prior to EAE induction, *Rela*-icKO mice were entirely protected against disease development, confirming the function of RelA in the early pathogenic process (Fig. 6 C). In contrast, when tamoxifen injections were initiated

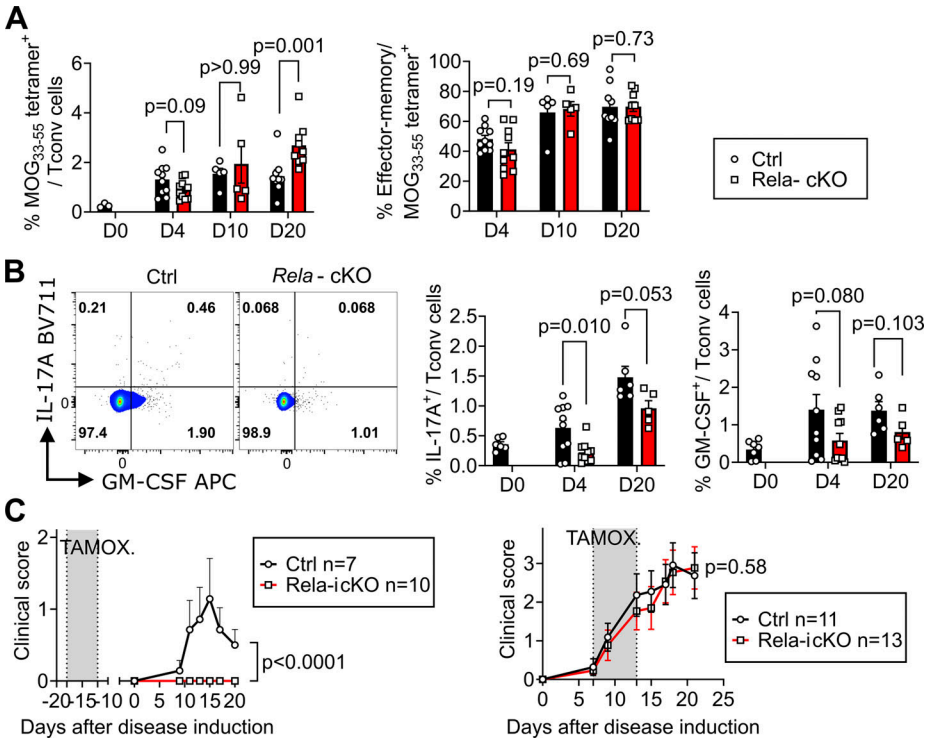

Figure 6. **RelA controls the priming phase but not the progression of EAE. (A and B)** EAE was induced in control ($CD4^{cre}$), *Rela*-cKO, and *Rel*-cKO mice. **(A)** Proportion of MOG_{33-55}-specific cells among Tconv (left) and their proportion of $CD62L^{-}CD44^{+}$ in dLN over time (right). Mean ± SEM of 3–10 mice/group/time point from two experiments are shown. **(B)** dLN cells were restimulated for 24 h with the MOG_{33-55} peptide and their expression of IL-17A and GM-CSF was assessed by FACS. Representative dot plots (left) and mean ± SEM of 3–10 mice/group/time point from two experiments are shown. **(C)** EAE was induced in control ($CD4^{cre\text{-}ert2}$) and *Rela*-icKO mice treated with tamoxifen from D−18 to D−12 (left, gray box) or from D7 to D13 (right). Clinical scores are shown (7–13 mice/group from *n* = 2 [left] or 3 [right] experiments). Mann–Whitney tests (A and B) and two-way ANOVA followed by Bonferroni's post-test (C) were used.

after the appearance of the first signs (from D7 on), the course of the disease was similar between control and *Rela*-deficient animals, thus demonstrating that Tconv cell–autonomous RelA was required for the initiation of the disease but dispensable for its progression. Collectively, this establishes RelA as a novel and critical regulator of Tconv function in autoimmunity through the regulation of TH17 differentiation in lymphoid and inflamed tissues.

c-Rel orchestrates the antitumor function of Tconv

In contrast to their deleterious role in autoimmunity, Tconv are currently emerging as critical actors of antitumor immunity. Therefore, we wondered whether our findings in the settings of EAE could be mirrored in cancer. To overcome the possible roles of NF-κB in $CD8^{+}$ T cells, we used again $CD4^{cre\text{-}ERT2}$ mice. Control ($CD4^{cre\text{-}ERT2}$), *Rela*, and *Rel*-icKO mice were transplanted with B16-OVA melanoma cells and treated with tamoxifen from D1 to D7. Intriguingly, the ablation of c-Rel led to a significant increase in tumor volume and weight, whereas RelA deletion had no impact (Fig. 7, A and B). We investigated the mechanism underlying enhanced growth by spectral FACS 19 days after tumor transfer. First, we observed that the total numbers of Tconv in the dLN and tumors were similar between strains (Fig. 7 C). Nevertheless, their phenotype was different in the absence of NF-κB. Indeed, in dLN, ablation of either *Rel* or *Rela* led to a modest but significant increase in the proportion of naive T cells but left the proportion of cytokine-producing cells following PMA-ionomycin restimulation unaltered (Fig. 7, D and E). Although impaired Tconv activation in dLN was observed in both *Rel*-icKO and *Rela*-icKO mice, only *Rel*-icKO animals displayed enhanced tumor burden. Thus, this role of NF-κB in dLN could not be the sole underlying mechanism of accelerated cancer progression, and it is likely that c-Rel also has an additional unique function in tumor tissues. In line with this, the increase in the proportion of naive-like Tconv was limited to *Rel*-icKO mice and occurred at the expense of $CD44^{high}CD62L^{low}$ TEM cells (Fig. 7 F). This was accompanied by a significant decrease in IFNγ, IL-2, TNF-α, and GzmB expression, highlighting defective Tconv function in situ (Fig. 7 G). In addition, we detected a trend toward a lower proportion of cytokine-expressing $CD8^{+}$ T cells in tumor tissues of *Rel*-icKO mice, suggesting an impaired CD4 > CD8 help (Fig. S5 A). Thus, c-Rel rather than RelA, was critical for the control of tumor growth by impacting $CD4^{+}$ Tconv both in dLN and tumor tissues.

To dissect the effects of c-Rel on the Tconv transcriptome, we performed scRNA-seq analysis of Tconv from control and *Rel*-icKO mice, 15 days after B16-OVA implantation. A total of 16,571 cells from tumors and dLN were successfully sequenced. As for EAE analyses, we first excluded Treg and non-T cell populations and reclustered cells according to the tissue (Fig. S5, B and C). In dLN, four main subsets were identified, with the vast majority of cells harboring a naive-like phenotype (Fig. S5, D and E). As

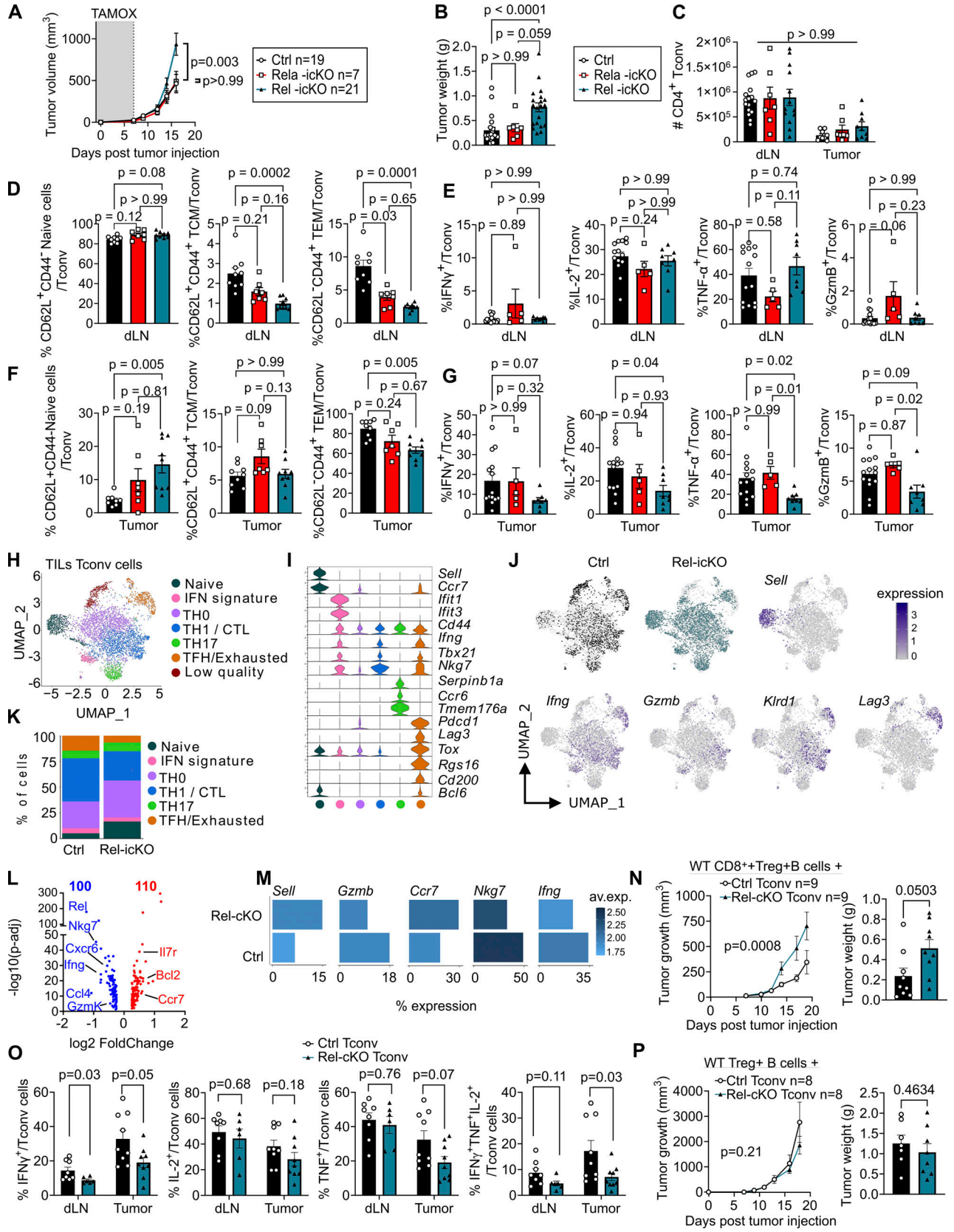

Figure 7. **c-Rel orchestrates Tconv function in the tumor microenvironment. (A–M)** Ctrl (CD4$^{cre\text{-}ert2}$), *Rela*-icKO, and *Rel*-icKO mice were treated with tamoxifen from D−1 to D7 (gray box) and transplanted with B16-OVA melanoma cells. **(A)** Tumor volume over time (n = 7–21 mice/group from four experiments). **(B)** Tumor weight at D19. **(C–G)** FACS analysis at D19 in dLN (C–E) and tumors (C, F, and G) without (C, D, and F) or with (E and G) PMA-ionomycin restimulation. The proportion of CD45$^+$TCRβ$^+$CD4$^+$CD8$^-$Foxp3$^-$ Tconv among total live cells and their expression of indicated markers are shown as mean ±

SEM of 5–14 mice/group from three experiments. **(H–M)** CD4+ T cells were sorted from the tumor at D15 and analyzed by scRNA-seq (performed once with 6–7 pooled mice/genotype). **(H)** UMAP representation of Seurat clusters. **(I)** Violin plot showing expression of selected cluster-defining genes. **(J)** Cell distribution between genotypes, and expression of selected markers projected on UMAP. **(K)** Distribution of the eight clusters in each genotype. **(L)** Volcano plot representation of DEGs (blue: downregulated, red: upregulated, P-adj cutoff <0.05). **(M)** Percentage and intensity of expression of selected genes in all Tconv. **(N–P)** *Rag2*$^{-/-}$ mice were reconstituted with Tconv, Treg, B cells, with (N and O) or without (P) CD8+ T cells, and transplanted with MC-38 cells. **(N)** Tumor growth (left) and weight at D19 (n = 9 mice/group from two experiments). **(O)** FACS analysis at D19 in dLN and tumors are shown as mean ± SEM of 6–9 mice/group from two experiments. **(P)** Tumor growth (left) and weight at D19 (n = 8 mice/group from two experiments). Two-way ANOVA followed by Bonferroni's post-test (A, N, and P), Kruskal–Wallis tests (B–G), and Mann–Whitney tests (O) were used.

expected, based on FACS analyses, *Rel*-icKO mice had slightly higher proportions of naive Tconv at the expense of the TH1 cell cluster (Fig. S5, F–H). This resulted in only 27 DEGs between the two genotypes (Fig. S5 H). Among tumor-infiltrating Tconv, seven clusters were identified, including a low-quality (low gene count, mtDNA^{high} [mitochondrial DNA], rRNA^{low} [ribosomal RNA]) cluster that was excluded from further analyses (Fig. 7, H and I). The naive-like cluster (*Ccr7*, *Sell*, *S1pr1*, and *Ly6c1*) was largely enriched (17% versus 5%) in *Rel*-deleted cells (Fig. 7, J and K; and Fig. S5 I). In contrast, subsets composed of TH1 and cytotoxic cells (*Ifng*, *Tbx21*, *Nkg7*, *Gzmb*, and *Klrd1*) and TFH and/or exhausted cells (*Pdcd1*, *Tox*, *Rgs16*, *Cd200*, *Lag3* with low expression of *Bcl6* and *Il21*) were largely impaired in the absence of c-Rel (Fig. 7, J–M). This decrease in exhausted and cytotoxic cells was further documented at the protein level by FACS analyses (Fig. S5 J). To understand whether this loss of differentiated cells resulted from increased apoptosis and/or decreased proliferation of *Rel*-deficient Tconv, we compared the enrichment of gene signatures related to these mechanisms in control and mutant cells but found no differences in these parameters between genotypes (Fig. S5 K). Taken together, this showed that c-Rel, rather than RelA, controlled the priming of TH1 and cytotoxic CD4+ T cells required for tumor control in vivo, despite minimal involvement in vitro. To unequivocally demonstrate that increased tumor growth in *Rel*-icKO animals relied on a Tconv cell–intrinsic role of c-Rel, we next applied a cell-transfer approach. *Rag2*-deficient mice were reconstituted with WT CD8+ T cells, Tregs, and B cells, as well as control or *Rel*-cKO CD4+ Tconv, and subsequently transplanted with MC38 colon adenocarcinoma cells. Again, we observed a dramatic acceleration of tumor growth in animals grafted with *Rel*-deficient Tconv (Fig. 7 N). This was associated with an impaired Tconv function, with a trend toward decreased IFNγ, TNF, and IL-2 expression in the tumor (Fig. 7 O). Overall, the proportion of polyfunctional IFNγ+TNF+IL-2+ Tconv was significantly impaired in the absence of c-Rel. Next, to investigate the link between Tconv and CD8+ T cells, we repeated the same Tconv transfer experiment but in the absence of exogenous CD8+ T cells. In this context, the ablation of Rel failed to modify tumor growth (Fig. 7 P). Thus, the antitumor function of c-Rel likely relied on a facilitated CD4 > CD8 help, rather than on an intrinsic cytotoxic function of Tconv.

As Tconv are involved in the response to checkpoint-blockade therapies, we next investigated whether c-Rel might be involved in their function in this context. Female control and *Rel*-icKO mice were transplanted with MC38 cells and subsequently treated with anti-PD-1 mAb. As for the B16-OVA model, Rel ablation drove enhanced tumor growth compared with controls treated with an isotype mAb (Fig. 8 A). Whereas PD-1 blockade drove a dramatic reduction in tumor growth in control animals, this therapeutic effect was abolished in *Rel*-icKO mice. These experiments revealed not only that intact CD4+ Tconv responses were integral to the response to anti-PD-1 mAbs but also that c-Rel activity is a crucial factor for this beneficial effect. We therefore examined the relevance of this observation in patients with cancer. Based on our scRNA-seq data (Fig. 7 L), we extracted a signature of nine genes downregulated in *Rel*-deficient tumor Tconv possessing human orthologs (Fig. 8 B). Using the iATLAS database (https://cri-iatlas.org), we investigated the expression of this signature using single-sample Gene Set Enrichment Analyses (ssGSEA) in cohorts of patients prior to treatment with PD-1–blocking agents, and its impact on the clinical response. In patients with metastatic cutaneous melanoma, bladder cancer, and stomach cancer, we found a statistical enrichment in the *Rel*-dependent signature in responders compared with non-responders (Fig. 8 C), which was associated with improved overall survival. Altogether, our data suggest that NF-κB, in particular through its c-Rel subunit, is a prime determinant of antitumor immunity through its role in Tconv.

Discussion

Almost four decades of literature have demonstrated the critical functions of NF-κB in a myriad of biological processes, especially in innate and adaptive immune responses. However, surprisingly, the selective and T cell autonomous contributions of each of the five subunits that compose the family are still largely unresolved; in particular those of RelA, which is ubiquitously expressed and widely accepted as a major orchestrator of gene expression profiles following immune cell stimulation. RelA was proposed to drive both *Ifng* and *Rorc* expression in mouse T cells (Balasubramani et al., 2010; Ruan et al., 2011), and recent CRISPR screening approaches unveiled its role in human Tconv proliferation and *Il2* expression (Schmidt et al., 2022; Shifrut et al., 2018). In this study, by employing two widely used animal models of autoimmunity and cancer, we demonstrate that RelA and c-Rel have distinct functions in Tconv depending on the disease context.

These conclusions were drawn following the use of cKO mouse models, which, unlike germline ablations, allowed cell type–restricted ablation of each gene. This was particularly important in the context of immune responses, as NF-κB subunits have been identified to exert critical roles in both innate and adaptive immunity. The results presented herein question some of the conclusions that were previously drawn from the

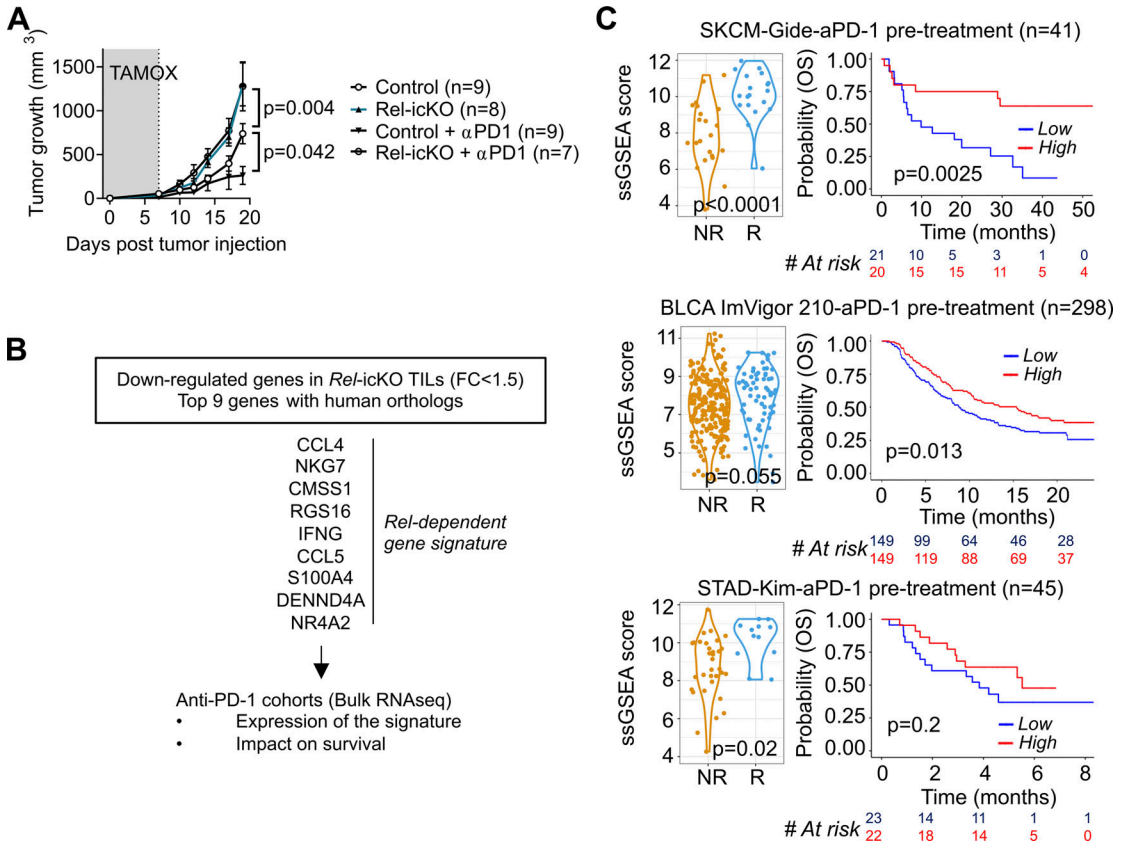

Figure 8. **c-Rel is required for the response to anti-PD-1 therapy. (A)** Control ($CD4^{cre\text{-}ert2}$) and *Rel*-icKO mice were treated with tamoxifen from D−1 to D−7 (gray box), transplanted with MC38 colon adenocarcinoma cells, and treated with anti-PD1 at D7, 9, and 11. Tumor volume over time (mean ± SEM from three experiments with 7–9 mice/group) is shown. **(B)** Identification of a *Rel*-dependent gene signature as described in Materials and methods. **(C)** ssGSEA scores (left panels) and Kaplan–Meier overall survival (OS) curves with the number of patients at risk shown below (right panels) in cohorts of patients with cutaneous melanoma (SKCM), bladder carcinoma (BLCA), and stomach adenocarcinoma (STAD). NR, non-responders; R, responders. Two-way ANOVA followed by Bonferroni's post-test (tumor volumes), Mann–Whitney tests (ssGSEA scores), and Log-rank tests (survival curves) were used.

study of germline KO animals and mutant patients. For instance, we showed here that RelA, rather than c-Rel, was critical for the acquisition of a cell-autonomous pathogenic TH17 profile and for the development of EAE. This result was surprising given previous literature implicating c-Rel in TH17 development and EAE pathogenesis. In vitro, both RelA and c-Rel can bind the *Rorc* promoter (Fig. S3 F and Ruan et al., 2011), but our data suggest that RelA is in fact the prominent subunit required for its expression. Similar conclusions could be drawn concerning proliferation; although c-Rel was important for Tconv proliferation in vitro, *Rela* ablation had a much greater impact in vivo during EAE. Our results also imply that protection of EAE in mice with germline ablation of *Rel* may rely on a Tconv cell–extrinsic mechanisms, such as dendritic cells or macrophages, which were shown to be dependent on c-Rel for their maturation and production of TH-inducing cytokines IL-12 and IL-23 (Hilliard et al., 2002; Visekruna et al., 2015; Zhang et al., 2017).

At steady-state and in autoimmunity, RelA appeared to have a more prominent role than c-Rel in shaping the transcriptome of Tconv. This function was achieved both through direct binding to target genes and through the induction of other transcription factors such as AP-1 family members. Downstream of MAPK signaling, AP-1 transcription factors have been implicated in T cell activation and IL-2 expression, in particular through interaction with NFAT and NF-κB members (McGuire and Iacobelli, 1997; Rincón and Flavell, 1994; Su et al., 1994). In addition, a number of AP-1 proteins such as BATF and JunB (both regulated by RelA, see Fig. S1 L) have been implicated in TH17 polarization (Schraml et al., 2009; Yamazaki et al., 2017), implying that RelA may regulate this subset both through direct regulation of *Rorc* but also through induction of additional transcription factors involved in the TH17 regulatory network (Ciofani et al., 2012). This was also corroborated by the protection of *Batf*- or *Junb*-deficient mice against EAE (Schraml et al., 2009; Yamazaki et al., 2017), similar to *Rela*-cKO animals. This establishes RelA as an apex regulator of gene expression in Tconv. However, c-Rel, but not RelA, was required for the antitumor function of Tconv. This critical observation not only reinforces the role of $CD4^+$ T cells in cancer immunity but also unravels a selective molecular mechanism orchestrating their accumulation and function in the tumor bed. Many different roles have been attributed to Tconv in limiting tumor growth, most notably the expression of inflammatory cytokines such as IFNγ, a help to $CD8^+$ T cells, and direct cytotoxicity against tumor cells through the secretion of perforin and granzymes. Strikingly, c-Rel seems to be involved in all these mechanisms

and thus could be proposed as a multifactorial regulator of antitumor immunity. Nevertheless, the protective role of c-Rel in Tconv was abrogated in the absence of CD8⁺ T cells, thus its function in the CD4 > CD8 help seems a prominent causative mechanism in cancer. As CD8⁺ T cells also appear to play pivotal functions in multiple sclerosis and its animal models (Saligrama et al., 2019; Steinman, 2001), it would also be relevant to investigate the role of NF-κB subunits in the CD4-CD8 relationship in EAE.

Tconv are also emerging as important actors in the response to immunotherapies such as chimeric antigen receptor (CAR) T cells or anti-PD-(L)1 checkpoint blockers, and it will be interesting to investigate the role of c-Rel in the clinical efficacy of these drugs. Our analyses of public transcriptomic data suggest that c-Rel activity is associated with good prognosis for the overall survival of cancer patients and their response to anti-PD-1 treatment.

The distinct roles of RelA and c-Rel in autoimmunity and cancer are obviously puzzling observations. Generally speaking, RelA and c-Rel seem to control Tconv activation in a similar manner, i.e., by controlling the transition from naive/early activated to effector (TH1, TH17, or Tc) T cells in both dLN and non-lymphoid tissues. However, the molecular basis underlying the selective function of these two transcription factors is still unclear. One explanation might be the existence of specific binding patterns to target genes. The definition of consensus binding sequences for RelA and c-Rel in Tconv, demonstrated by us and others (Lévy et al., 2021; Oh et al., 2017), resulted from ChIP-Seq experiments conducted in vitro, which prevent drawing definitive conclusions in vivo. Moreover, systematic analyses of NF-κB subunits binding in lymphoma cell lines revealed similar consensus binding sequences (de Oliveira et al., 2016; Zhao et al., 2014). This was recently confirmed in primary B cells, in which selective function of RelA and c-Rel appeared to rely on differences in the kinetics of expression and activation of the subunits themselves rather than on different binding sequences (Zhao et al., 2023). Thus, it is unlikely that a simple separation of DNA binding by RelA and c-Rel could explain this phenotypic discrepancy, although there is still a rationale for additional investigation in vivo. Moreover, it remains possible that the dimer composition and/or their association with other transcriptional regulators could impact the preferred binding motif, as shown in tumor cell lines (Wong et al., 2011). Another possibility could be the selective activation of RelA and c-Rel in the CNS and tumor-infiltrating Tconv, respectively. This would rely on differential types, duration, and strength of stimulation of surface receptors (TCR, CD28, TNFR superfamily members, and other cytokine receptors) that would drive the preferential translocation and DNA binding of a given subunit, or the association with other transcription factors. This concept of "activation modules" has been elegantly approached by Hoffmann and colleagues, who showed, in primary macrophages, that RelA activation and expression of target genes were dependent on such dynamic features (Adelaja et al., 2021; Cheng et al., 2021). Added to the complexity of dimer composition and affinity for target genes (Brignall et al., 2019), the specificity of NF-κB subunits in inflammation likely relies on a series of different parameters. Such analyses conducted in Tconv, concomitantly for RelA and c-Rel, would undoubtedly provide mechanistic insights into the distinct regulation of disease outcomes by NF-κB subunits.

In addition to these biological insights, our observations have strong therapeutic implications. Extensive literature highlighting the deleterious roles of (canonical) NF-κB in autoimmunity and cancer has led to the development of inhibitors of upstream kinases of the pathway, in particular inhibitor of NF-κB kinase (IKK) inhibitors (Gilmore and Herscovitch, 2006; Lalle et al., 2021b). Nevertheless, despite promising preclinical results in murine models of EAE and transplanted melanoma among others, very few compounds progressed to advanced clinical trials because of lack of efficacy and/or high toxicity (Baud and Karin, 2009). One may reason that these failures may in part be due to the absence of selective targeting of specific NF-κB subunits. Our data may thus pave the way toward more potent agents. In autoimmunity, the time-controlled inhibition of RelA appears as a promising solution, at least in the early stages of the disease or in remitting phases of relapsing/remitting MS. Although only a few chemical inhibitors have so far been described, other approaches such as siRNA targeting *Rela*, may be effective (Yan et al., 2016). Ideally, such inhibitors should be directly targeted to T cells, for instance, by using antibody–drug conjugates. In cancer, we and others have shown that systemic inhibition of c-Rel restricts tumor growth in mouse models by targeting the activity of Treg cells and/or myeloid-derived suppressor cells (Grinberg-Bleyer et al., 2017; Li et al., 2020). Our results suggest an alternative therapeutic approach consisting of activating c-Rel in Tconv. This could for instance be achieved by using gene-edited cellular products. A proof-of-concept approach using TCR-transgenic CD8⁺ T cells expressing constitutively active IKKβ, or deficient for A20, in murine cancer, provided a rationale for such strategies (Evaristo et al., 2016; Giordano et al., 2014). Similarly, a gain-of-function screening approach recently highlighted that ectopic expression of lymphotoxin-β receptors in CAR-T cells improved tumor control in an NF-κB–dependent manner (Legut et al., 2022). It would therefore be interesting to investigate the putative superiority of *Rel*-overexpressing TCR-T cells or CAR-T cells, as recently shown with BATF-overexpressing CD19-CAR T cells (Seo et al., 2021).

Materials and methods

Mice

Rel- and *Rela*-Floxed mice were previously described (Heise et al., 2014). $CD4^{cre}$ (Tg[CD4-cre]^{1Cwi}) and $CD4^{cre\text{-}ERT2}$ (B6[129X1]-Tg[Cd4-cre/ERT2]11Gnri/J) were purchased from the Jackson Laboratory and backcrossed to C57Bl/6J at least 10 times. Controls ($CD4^{cre}$ and $CD4^{cre\text{-}ERT2}$) and cKO/icKO mice were either true littermates or were age- and sex-matched. *Rag2*$^{-/-}$ in a C57Bl/6J background and C57BL/6 CD45.1 (*Ptprc*^{a} *Pepc*^{b}/BoyJ) mice were purchased from Charles River Laboratories France. Mice were bred and used in specific pathogen–free conditions at the Cancer Research Center of Lyon (CRCL) animal facility (plateforme du petit animal du CRCL [P-PAC]). Animals were housed in individually ventilated cages with temperature-

controlled conditions under a 12-h light/dark cycle with free access to drinking water and food. Adult (6–30 wk old) male or female mice were used for all experiments. Studies were conducted in accordance with the animal care guidelines of the European Union and French laws. Protocols were validated by the local Animal Ethics Evaluation Committee (committee C2A15) (Protocols CLB-2018052217411370 and CLB-2019061914498113). The authors complied with the Animal Research: Reporting of In Vivo Experiments guidelines.

Human subjects

Blood samples from healthy volunteers were obtained through the French Blood Bank (Etablissement Français du Sang, agreement 22-093). The studies were conducted in accordance with the local legislation and institutional requirements. Clinical and RNA-seq data from cancer patients were publicly available (https://cri-iatlas.org).

Cell lines, transplantation, and immunotherapy

MC-38 cells were a gift from Benoit Salomon (Centre d'Immunologie et des Maladies Infectieuses [CIMI-Paris], Paris, France). B16F10-OVA cells were made in-house by transfection of the full-length ovalbumin pcDNA3-OVA plasmid (64599; Addgene) in B16F10 cells (American Tissue Culture Collection), followed by selection in medium containing 500 µg/ml Neomycin (Sigma-Aldrich) and validation by PCR and functional assays. Cell lines were maintained in DMEM (Thermo Fisher Scientific) +10% fetal bovine serum (FBS, Thermo Fisher Scientific). 2×10^5 MC38 or 3.5×10^5 B16F10-OVA cells diluted in 50 µl ice-cold sterile PBS1X were injected subcutaneously into the shaved flank of each mouse. After 7 days, tumor size was monitored every other day with a Caliper. Tumor volume was obtained by using the formula: width^2 × length. Anti-PD-1 (RMP1-14) and rat isotype control mAbs were obtained from BioXCell. Mice received intraperitoneal injections of 200 µg of mAb diluted in PBS1X.

EAE

Mice were injected subcutaneously in each flank with 50 µg of MOG_{35-55} peptide (SB023; Smart Biosciences) emulsified in 100 µl of complete Freund's adjuvant (Sigma-Aldrich) supplemented with 243 µg of heat-killed *Mycobacterium tuberculosis* H37Ra (2311; Difco-BD Bioscience). *Bordetella pertussis* toxin (200 ng/injection, Enzo) was injected intravenously at the time of immunization and 2 days later. Disease severity was evaluated every other day following an established scoring system in a semiblinded fashion: 0, no clinical sign; 1, limp tail; 2, limp tail, impaired righting reflex, and paresis of one limb; 3, hindlimb paralysis; 4, complete hindlimb and partial forelimb paralysis; to 5, moribund/death. A score of 5 was permanently attributed to dead animals.

Mixed BM chimera

BM cells were isolated from tibia and femur of donor mice. Red blood cells were lysed and cells were enumerated. BM mixes were made with $^1/_3$ WT CD45.1 BM and $^2/_3$ CD45.2 BM of interest ($CD4^{cre}$, $CD4^{cre}$ $Rela^{flox/flox}$ or $CD4^{cre}$ $Rel^{flox/flox}$). Recipient mice were sublethally irradiated (7 Gy) and transplanted intravenously (retro-orbital sinus) with 10×10^6 BM cells. Mice were given Neomycin (200 ng/ml) in drinking water for 10 days. Tissues were harvested 8 wk after reconstitution for subsequent analyses.

T/B cell reconstitution of *Rag2*$^{-/-}$ mice

Spleen and LNs of donor mice were dissected, and soaked in two baths of 70% ethanol and two baths of PBS1X. Tconv were isolated by using the $CD4^+$ T cell Isolation Kit, mouse (Miltenyi Biotec) according to the manufacturer's protocol together with anti-CD25-biotin antibody (7D4; BD) to deplete Treg cells.

Tregs and B cells were isolated through positive selection by labeling with anti-CD25-biotin antibody and anti-CD19-biotin antibody, respectively, followed by incubation with anti-biotin microbeads (Miltenyi Biotec). $CD8^+$ T cells were isolated using the MojoSort Mouse CD8 T cell Isolation Kit (Biolegend) according to the manufacturer's protocol. 2.5×10^6 Tconv, 0.6×10^6 Treg, 2.5×10^6 B cells, with or without 2×10^6 $CD8^+$ T cells, were injected intravenously to anesthetized *Rag2*$^{-/-}$ mice. MC-38 cells were transplanted 7 days later.

Preparation of cell suspensions

Single-cell suspensions from LN and spleens were obtained by mechanical dilaceration in FACS Buffer (PBS1X + 2% FBS, 2 mM EDTA) with glass slides, strained, washed in complete RPMI, and enumerated.

For EAE experiments, mice were anesthetized with a mixture of ketamine and xylazine and perfused with ice-cold PBS1X. Draining (brachial) LNs, brain, and spinal cord were harvested in ice-cold NaCl solutions. Brains and spinal cords were cut into small pieces and digested in RPMI 1640 (Gibco) supplemented with 1 mg/ml collagenase type IV (Sigma-Aldrich), 500 µg/ml DNase I (Sigma-Aldrich) for 30 min at 37°C followed by mechanical desegregation. Reactions were stopped by the addition of 15 ml PBS1X containing 5 mM EDTA. The solution was passed through a 70-µm cell strainer and residual solid pieces were mechanically disrupted. After centrifugation, cell pellets were resuspended in 8 ml of Percoll 40% (Sigma-Aldrich) and then laid on 4 ml Percoll 80% in a 15 ml polypropylene tube. Tubes were spun at 2,500 rpm for 20 min at room temperature (RT). Mononuclear cells were collected from the interface of the 40:80% Percoll gradient, washed in complete RPMI, and enumerated.

Tumors were cut into small pieces and digested in RPMI 1640 (Gibco) supplemented with 1 mg/ml collagenase type IV (Sigma-Aldrich), 250 µg/ml DNase I (Sigma-Aldrich) for 25 min at 37°C followed by mechanical desegregation. Reactions were stopped by the addition of 15 ml PBS1X containing 5 mM EDTA. The solution was passed through a 70-µm cell strainer and residual solid pieces were mechanically disrupted. After centrifugation, cell pellets were resuspended in 8 ml of Percoll 44% (Sigma-Aldrich) and then laid on 4 ml Percoll 67% in a 15 ml polypropylene tube. Tubes were spun at 2,500 rpm for 20 min at RT. Mononuclear cells were collected from the interface of the 44:67% Percoll gradient, washed in complete RPMI, and enumerated.

NF-κB ablation in human T cells

Peripheral blood mononuclear cells were isolated by Ficoll density gradient centrifugation, and red blood cells were lysed with ammonium–chloride–potassium lysis buffer. Naive CD4$^+$ T cells were isolated using the EasySep Human Naive CD4 T cell Isolation kit II (Stemcell) according to the manufacturer's protocol. Cells were enumerated and resuspended at 1 × 10^6 cells/ml in complete RPMI 1640 W/HEPES W/GLUTAMAX-I (Thermo Fisher Scientific, supplemented with 10% FBS; penicillin/streptomycin; non-essential amino acids; sodium pyruvate and β-mercaptoethanol) with human IL-2 (25 U/ml; Miltenyi) and Dynabeads CD3/CD28 (Thermo Fisher Scientific, 1 bead:4 T cells). Cells were cultured for 3 days. RNP complexes were prepared by mixing crRNA (IDT), ATTO550-tracrRNA (IDT), CAS9 (Truecut v2 cas9; Thermo Fisher Scientific), and electroporation enhancers (IDT) at an equimolar ratio in a final solution at 7.5 nmol/ml. CRISPR-RNA (crRNA) and trans-activating crRNA (tracrRNA) were incubated 5 min at 95°C then 15 min at 37°C. Then CAS9 was added and solutions were incubated for 15 min at 37°C. Finally, an electroporation enhancer was added to the mix. Dynabeadds were removed and cells were washed and resuspended at 14 × 10^6 cells/ml in Buffer T (Neon transfection system, Thermo Fisher Scientific). Cells and RNP complexes were mixed so that 1.3 × 10^6 cells could be electroporated in a 100 µl Neon Tip with 50 pmol of RNP. Electroporation was performed with the Neon transfection system (1600V, 10 ms, 3 pulses). Then cells were put in 1.9 ml of complete RPMI with IL-2 (20 U/ml) and Dynabeads CD3/CD28 (1 bead:10 T cells). Cells were cultured for 3 days, washed, and stained with DAPI in FACS Buffer. DAPI$^-$ ATTO550$^+$ cells were sorted on a FACS ARIA II system and used for subsequent assays.

In vitro TH polarization assays

Naive CD4$^+$ T cells were negatively isolated using the Naive CD4$^+$ T cell Isolation Kit (Miltenyi Biotec). Cells were labeled using the CellTrace Violet Cell Proliferation Kit (CTV; Thermo Fisher Scientific). 3 × 10^4 cells were stimulated with different doses of T cell–depleted mitomycin C–treated Ly5.1 splenocytes and soluble anti-CD3ε (clone 145-2C11; BioXcell): 6 × 10^4 splenocytes + 2 µg/ml anti-CD3ε (high stim), 1.5 × 10^4 splenocytes + 0.5 µg/ml anti-CD3ε (medium stim), or 0.5 × 10^4 splenocytes + 0.2 µg/ml anti-CD3ε (low stim), in complete IMDM (Thermo Fisher Scientific, 10% FBS, 25,000 U Penicillin/Streptomycin, 10 mM sodium pyruvate, non-essential amino acids, and 50 µM 2-Mercaptoethanol). The culture medium was supplemented as follows: TH1: 20 ng/ml mIL-12 (Peprotech), 10 ng/ml mIL-2 (Miltenyi), 2 µg/ml anti-mouse IL-4 (clone 11B11; BD Biosciences); TH2: 30 ng/ml mIL-4 (Peprotech), 2 µg/ml anti-mouse IFNγ (clone XMG1.2; BD Biosciences), 2 µg/ml anti-mouse IL-12 (clone C17.8; BD Biosciences); 10 ng/ml mIL-2; TH17: 1 ng/ml hTGF-β, 20 ng/ml mIL-6 (Peprotech), 2 µg/ml anti-mouse IFNγ, 2 µg/ml anti-mouse IL-4; inflammatory TH17: same as TH17 with 5 ng/ml mIL-1β (Peprotech); 5 ng/ml hIL-23 (Peprotech) and 2 µg/ml anti-mouse IL-2 (clone JES6-1A12, Biolegend). After 4 days of culture, proliferation and subset-specific transcription factors and cytokine expression were assessed by FACS.

Flow cytometry

For cytokine analysis by FACS, single-cell suspensions were stimulated for 4 h at 37°C with 50 ng/ml PMA (Sigma-Aldrich), 1 µg/ml ionomycin (Sigma-Aldrich), and 1X Protein Transport Inhibitor containing Brefeldin A (BD GolgiPlug). Cells were washed in PBS1X and stained with a viability marker for 10 min at RT in the dark. Cells were washed in PBS1X and incubated with 50 µl surface marker antibody mix for 20 min a 4°C in the dark. Cells were then washed in PBS1X and fixed and permeabilized using the eBioscience Foxp3/Transcription Factor Staining Buffer Set (Thermo Fisher Scientific) according to the manufacturer's instructions. Cells were washed and incubated with the intracellular marker antibody mix for 20 min at 4°C in the dark, washed in permeabilization buffer, and resuspended in FACS Buffer.

When GFP fluorescence was analyzed, after cell surface labeling, cells were fixed by using 2% paraformaldehyde (MPbio) for 30 min (instead of the eBioscience Foxp3/Transcription Factor Staining Buffer Set) and then washed twice with wash buffer from the eBioscience Foxp3/Transcription Factor Staining Buffer Set. Then for intracellular labeling, cells were washed and incubated with the intracellular marker antibody mix for 30 min at 4°C in the dark, washed in permeabilization buffer, and resuspended in FACS Buffer. Occasionally, antibodies coupled to biotin were used. In this case, there was an extra step of staining with fluorochrome-coupled streptavidin (in FACS buffer if cell surface labeling or wash buffer if intracellular labeling).

The complete list of antibodies can be found in Table S1. Acquisition was performed on a LSR Fortessa (BD Biosciences) or an Aurora spectral cytometer (Cytek). Data were analyzed with FlowJO software V10.7.2 (Tree Star, https://www.flowjo.com).

Luxol Fast Blue coloration

To estimate the level of demyelination in the white matter of EAE mice, 5 µm spinal cord sections were first deparaffinized, hydrated, and then incubated in Luxol Fast Blue solution overnight at 58°C. Excess coloration was then rinsed off in 95% ethanol and distilled water baths. Subsequently, sections were differentiated in 0.05% lithium carbonate solution for 30 s and then in 70% ethyl alcohol solution for 30 s. Sections were further rinsed in distilled water and counterstained with nuclear red solution. After two additional rinses in distilled water, spinal cord sections were dehydrated in successive baths of ethyl alcohol and slides mounted in cover-quick mounting medium.

Immunofluorescence assays and data analysis

Mice were perfused with 20 ml PBS1X and then with 10% formalin. Spinal cords were fixed in 4% formalin for 24 h and then kept in 70% EtOH. 25-µm-thick slices from the thoracic-lumbar spinal cords were generated using a sliding microtome with a 100-µm interval between each section.

Slices were first incubated for 40 min at RT with a blocking solution made of PBS-Triton 0.1% (X100; Sigma-Aldrich), 5% BSA (A3294; Sigma-Aldrich), 5% goat serum (S-1000-20; Vector Laboratories), and 3% mouse serum. Subsequently, the slices were incubated overnight at 4°C under mild agitation with the

primary chick anti-mouse Iba1 antibody (234 006; Synaptic System) diluted 1:300 in PBS-Triton 0.01–0.5% NGS-0.3% mouse serum-0.5% BSA. The next day, slices were washed (three times for 5 min) with PBS-Triton 0.1% and incubated for 2 h at RT under mild agitation with the secondary antibody Alexa488 goat anti-chicken IgG (A11039; Invitrogen) diluted 1:500 in PBS-Triton 0.01%. Slices were then washed and incubated for 20 min at RT under mild agitation with Fluoromyelin (F34652; Invitrogen) (Monsma and Brown, 2012) diluted 1:300 in PBS-Triton 0.01%. After washing, slices were incubated with DAPI (28718-90-3; Merk) diluted 1:2,000 in PBS and mounted in Fluoromount medium (00-4958-02) on microscope slides.

7–20 spinal cord slices per mouse were acquired using a 3DHistec Panoramic 250 slide scanner (3DHistec Ltd). Quantification of Iba1 and Fluoromyelin staining was performed using the QuPath v0.4.3 software. Cross-section perimeters were first outlined based on the DAPI signal to obtain the total areas for each section. Then, for Iba1 staining, the same threshold for positive signal detection was applied to all the slides. The threshold was set with a moderate resolution (2.60 µm/px) using a Gaussian prefilter to calculate the surface occupied by Iba1$^+$ signal for each slice. A similar procedure was performed to calculate Fluoromyelin staining.

Bulk RNA-seq and analyses

RNA from 1 to 2 million Tconv was isolated with Nucleospin RNA extraction kits (Macherey Nagel) and libraries were prepared using an Illumina TruSeq Library Kit and sequenced by an Illumina NovaSeq instrument. Reads were aligned on reference genomes (mm10 for mouse data, GRCh38 for human data) and DEGs were calculated with DESeq2. Heatmaps were created with Morpheus (Morpheus [https://broadinstitute.org]). GSEA was computed using the GSEA application and Gene Ontology, KEGG, Hallmarks, and c7 packages. Comparison with public ChIP-Seq data (GSE132476) was done after peak annotation with the library org.Mm.eg.db and the function annotatePeak with a tssRegion range defined as (–10,000, 5,000). Given that one gene can have multiple binding sites, we used the aggregate function to count the number of occurrences of a target gene and extract target gene names without duplicates.

scRNA-seq and analyses

CD4$^+$ T cells were FACS sorted (BD ARIA 3) from tumors, brains, and dLNs. For EAE experiments, five CD4^{cre}, six Rela-cKO, and six Rel-cKO mice were used. For tumor experiments, six CD4$^{cre\text{-}ert2}$ and seven Rel-icKO mice were used. 3,000–4,000 cells/experimental group were pooled from independent mice, barcoded using the CellPlex technology (10X Genomics), and encapsulated using the Chromium iX (10X Genomics) on Chip G according to manufacturer's instructions. Libraries were prepared using the Chromium Single Cell 3′ Library v3.1 kit following 10X Genomics recommendations and sequenced on an Illumina NovaSeq 6000. Reads were demultiplexed and aligned with CellRanger software (10X Genomics). Expression data were computed from Fastq files with CellRanger (v6.1.1 for CNS samples and v7.0.0 for tumor infiltrating lymphocyte [TIL] samples). Each time, the mouse reference genome was used (refdata-gex-mm10-2020-A). Data were loaded into a Seurat object by keeping cells with more than 100 detected genes and genes found in more than two cells. Cells with <200 or >5,000 (cancer) or 6,000 (EAE) detected genes, or <5% (EAE) or 10% (cancer) of reads from mitochondrial genes were filtered out. Data were then normalized with the LogNormalize function from Seurat and scaled. We selected the top 1,000 most variable genes using the FindVariableFeatures function and the vst option. All cells were annotated with the ProjecTILS package (v3.0.0) and the make_projection function. We removed Tregs as cells annotated as such by ProjecTILS and presenting a Foxp3 expression >0. Next, dimensionality reduction was performed using principal component analysis, retaining 10 axes for EAE data and 40 for cancer data. Each dataset was then clustered using the Leiden algorithm with a resolution of 0.8 for EAE and 0.5 for cancer. Marker genes were extracted with the FindAllMarkers function from Seurat, keeping only positive genes with a minimum fraction of expressing cells of 0.5. Enriched pathways were computed with either the EnrichR or the UCell packages. DEGs between groups were identified using the FindMarkers function from Seurat, employing the model-based analysis of single-cell transcriptomics algorithm. For creating the c-Rel–dependent Tconv gene signature, only downregulated genes (positively regulated by c-Rel) were considered. Genes were sorted in descending order of adjusted P values and the first top 10 genes were used in the signature (excluding *Rel* itself). Mouse gene symbols were converted to human symbols using R package biomartR (v 2.52.0). Immune checkpoint inhibitors studies with RNA-seq data were retrieved from CRI iAtlas portal (https://isb-cgc.shinyapps.io/iatlas/) for several cancer types. To evaluate the prognosis potential of our homemade signature, an ssGSEA score was calculated using in-house function. For survival analyses, patients were stratified in groups based on median ssGSEA score. Kaplan–Meier curves were created using R package survival (v 3.4-0).

Western blot

Total lysates were extracted using radioimmunoprecipitation assay buffer and protease inhibitors (Sigma-Aldrich) with SDS. Protein concentration was quantified using BCA assay (Thermo Fisher Scientific). 20 µg protein extracts were run in 10% polyacrylamide gels (BioRad) and transferred onto polyvinylidene difluoride membranes using a TransBlot Turbo apparatus (Bio-Rad). Membranes were first blocked with Tris-buffered saline with 0.1% Tween 20 (TBS-T) + milk 5% for 45 min at RT, then incubated overnight at 4°C with the antibodies of interest diluted in TBS-T + milk 2.5%. The next morning, membranes were washed three times with TBS-T for 10 min and incubated with secondary antibodies diluted in TBS-T + milk 2.5% for 1 h at RT. Finally, membranes were washed four times with TBS-T for 10 min, soaked in Luminata Forte or Luminata Classico (Merck Millipore) buffer for 1 min, and revealed.

Antibodies used are available in Table S1.

Statistics

Statistics were performed using GraphPad Prism Software v9 (https://www.graphpad.com/scientific-software/prism/). Following assessment of the distribution, the following tests were

used: for FACS data and tumor weights, two-tailed Mann–Whitney or paired Student's *t* tests (when two groups) and Kruskal–Wallis (when three groups) tests were used. For tumor volumes and EAE score analyses, two-way ANOVA followed by Bonferroni post-test was used.

Online supplemental material

Fig. S1 shows FACS phenotyping of control and cKO mice at steady-state, FACS phenotyping of mixed BM chimeras, and analyses of mouse RNA-seq data. Fig. S2 shows analyses of human RNA-seq data. Fig. S3 shows mouse TH polarization assays, analysis of public RelA ChIP-Seq data, and analysis of myeloid cell activation during EAE. Fig. S4 shows analyses of scRNA-seq and FACS data in EAE, shows the role of RelA in CD8$^+$ T cells in EAE, and the efficiency of tamoxifen-induced RelA ablation in icKO mice. Fig. S5 shows analyses of scRNA-seq and FACS data in cancer. Table S1 details all the antibodies used in the study.

Data availability

Sequencing data have been deposited to the Gene Expression Omnibus database (GSE239704). All analyzed data are available in the figures. All raw data are available upon reasonable request addressed to yenkel.grinberg-bleyer@inserm.fr.

Acknowledgments

We are grateful to all members of the team for their technical help and constructive discussions; to the staff of the core facilities at CRCL for their expertise; to the administrative support staff of CRCL; and to Brigitte Manship for critical reading of the manuscript. We thank the National Institutes of Health Tetramer Core Facility (Atlanta, GA, USA) for providing tetramers.

This work was supported by the Centre National de la Recherche Scientifique/Institut National de la Santé et de la Recherche Médicale ATIP-Avenir young investigator program, the Labex DEVweCAN (ANR-10-LABX-0061), and the ARSEP Foundation, to Y. Grinberg-Bleyer. A. Voisin was supported by a postdoctoral fellowship from the ARC Foundation. P. Stéphan was supported by a doctoral fellowship from the Fondation pour la Recherche Médicale.

Author contributions: Y. Grinberg-Bleyer and S. Ghosh conceptualized the project. G. Lalle and R. Lautraite established methodology, designed and performed experiments, and analyzed data. K. Bouherrou, A. Pignata, A. Voisin, J. Twardowski, M. Perrin-Niquet, P. Stéphan, S. Durget, L. Belgarbi Dutron, N. Davoust, T.S. Postler, and J. Zhao performed experiments and analyzed data. M. Plaschka, L. Tonon, M. Ardin, C. Degletagne, and A. Viari provided methodological insights, curated and analyzed sequencing data. C. Caux, J. Caramel, S. Dalle, P.A. Cassier, U. Klein, and M. Schmidt-Supprian provided essential resources. R. Liblau analyzed data. Y. Grinberg-Bleyer supervised the work, secured funding, designed experiments, analyzed data, and wrote the paper with contributions from G. Lalle, R. Lautraite, and R. Liblau.

Disclosures: P. Cassier reported "other" from Abbvie, Amgen, Alligator, Blueprint, Boehringer Ingelheim, Daiichi Sankyo, Astrazeneca, C4 Therapeutics, Exelixis, Molecular Partners, Pierre Fabre, Relay, Sotio, Tango, GSK, Merck Sharp Dohme, Lilly/Loxo, Novartis, Roche/Genentech, Taiho, Transgene, and Toray; personal fees from BMS, OSE, and Brenus; and non-financial support from Debio outside the submitted work. R. Liblau reported personal fees from Novartis, Biogen, Sanofi-genzyme, and Vida Venture; non-financial support from Novo Nordisk; and grants from Roche, Population Bio, and BMS outside the submitted work. No other disclosures were reported.

Submitted: 1 August 2023
Revised: 30 January 2024
Accepted: 13 March 2024

References

Adelaja, A., B. Taylor, K.M. Sheu, Y. Liu, S. Luecke, and A. Hoffmann. 2021. Six distinct NFκB signaling codons convey discrete information to distinguish stimuli and enable appropriate macrophage responses. *Immunity*. 54:916–930.e7. https://doi.org/10.1016/j.immuni.2021.04.011

Badran, Y.R., F. Dedeoglu, J.M. Leyva Castillo, W. Bainter, T.K. Ohsumi, A. Bousvaros, J.D. Goldsmith, R.S. Geha, and J. Chou. 2017. Human RELA haploinsufficiency results in autosomal-dominant chronic mucocutaneous ulceration. *J. Exp. Med.* 214:1937–1947. https://doi.org/10.1084/jem.20160724

Balasubramani, A., Y. Shibata, G.E. Crawford, A.S. Baldwin, R.D. Hatton, and C.T. Weaver. 2010. Modular utilization of distal cis-regulatory elements controls Ifng gene expression in T cells activated by distinct stimuli. *Immunity*. 33:35–47. https://doi.org/10.1016/j.immuni.2010.07.004

Barnes, S.E., Y. Wang, L. Chen, L.L. Molinero, T.F. Gajewski, C. Evaristo, and M.-L. Alegre. 2015a. T cell-NF-κB activation is required for tumor control in vivo. *J. Immunother. Cancer*. 3:1. https://doi.org/10.1186/s40425-014-0045-x

Barnes, S.E., Y. Wang, L. Chen, L.L. Molinero, T.F. Gajewski, C. Evaristo, and M.L. Alegre. 2015b. T cell-NF-κB activation is required for tumor control in vivo. *J. Immunother. Cancer*. 3:1. https://doi.org/10.1186/s40425-014-0045-x

Baud, V., and M. Karin. 2009. Is NF-kappaB a good target for cancer therapy? Hopes and pitfalls. *Nat. Rev. Drug Discov.* 8:33–40. https://doi.org/10.1038/nrd2781

Beaussant-Cohen, S., F. Jaber, M.J. Massaad, S. Weeks, J. Jones, M.F. Alosaimi, J. Wallace, W. Al-Herz, R.S. Geha, and J. Chou. 2019. Combined immunodeficiency in a patient with c-Rel deficiency. *J. Allergy Clin. Immunol.* 144:606–608.e4. https://doi.org/10.1016/j.jaci.2019.05.003

Beg, A.A., W.C. Sha, R.T. Bronson, S. Ghosh, and D. Baltimore. 1995. Embryonic lethality and liver degeneration in mice lacking the RelA component of NF-kappa B. *Nature*. 376:167–170. https://doi.org/10.1038/376167a0

Betz, B.C., K.L. Jordan-Williams, C. Wang, S.G. Kang, J. Liao, M.R. Logan, C.H. Kim, and E.J. Taparowsky. 2010. Batf coordinates multiple aspects of B and T cell function required for normal antibody responses. *J. Exp. Med.* 207:933–942. https://doi.org/10.1084/jem.20091548

Borst, J., T. Ahrends, N. Bąbała, C.J.M. Melief, and W. Kastenmüller. 2018. CD4$^+$ T cell help in cancer immunology and immunotherapy. *Nat. Rev. Immunol.* 18:635–647. https://doi.org/10.1038/s41577-018-0044-0

Brignall, R., A.T. Moody, S. Mathew, and S. Gaudet. 2019. Considering abundance, affinity, and binding site availability in the NF-κB target selection puzzle. *Front. Immunol.* 10:609. https://doi.org/10.3389/fimmu.2019.00609

Chen, G., K. Hardy, E. Pagler, L. Ma, S. Lee, S. Gerondakis, S. Daley, and M.F. Shannon. 2011. The NF-κB transcription factor c-Rel is required for Th17 effector cell development in experimental autoimmune encephalomyelitis. *J. Immunol.* 187:4483–4491. https://doi.org/10.4049/jimmunol.1101757

Cheng, Q.J., S. Ohta, K.M. Sheu, R. Spreafico, A. Adelaja, B. Taylor, and A. Hoffmann. 2021. NF-κB dynamics determine the stimulus specificity of epigenomic reprogramming in macrophages. *Science*. 372:1349–1353. https://doi.org/10.1126/science.abc0269

Christophersen, A., E.G. Lund, O. Snir, E. Solà, C. Kanduri, S. Dahal-Koirala, S. Zühlke, Ø. Molberg, P.J. Utz, M. Rohani-Pichavant, et al. 2019. Distinct

phenotype of CD4+ T cells driving celiac disease identified in multiple autoimmune conditions. *Nat. Med.* 25:734–737. https://doi.org/10.1038/s41591-019-0403-9

Ciofani, M., A. Madar, C. Galan, M. Sellars, K. Mace, F. Pauli, A. Agarwal, W. Huang, C.N. Parkhurst, M. Muratet, et al. 2012. A validated regulatory network for Th17 cell specification. *Cell*. 151:289–303. https://doi.org/10.1016/j.cell.2012.09.016

Clavijo, P.E., and K.A. Frauwirth. 2012. Anergic CD8+ T lymphocytes have impaired NF-κB activation with defects in p65 phosphorylation and acetylation. *J. Immunol.* 188:1213–1221. https://doi.org/10.4049/jimmunol.1100793

Codarri, L., G. Gyülvészi, V. Tosevski, L. Hesske, A. Fontana, L. Magnenat, T. Suter, and B. Becher. 2011. RORγt drives production of the cytokine GM-CSF in helper T cells, which is essential for the effector phase of autoimmune neuroinflammation. *Nat. Immunol.* 12:560–567. https://doi.org/10.1038/ni.2027

Cohen, M., A. Giladi, O. Barboy, P. Hamon, B. Li, M. Zada, A. Gurevich-Shapiro, C.G. Beccaria, E. David, B.B. Maier, et al. 2022. The interaction of CD4+ helper T cells with dendritic cells shapes the tumor microenvironment and immune checkpoint blockade response. *Nat. Cancer*. 3:303–317. https://doi.org/10.1038/s43018-022-00338-5

Comrie, W.A., A.J. Faruqi, S. Price, Y. Zhang, V.K. Rao, H.C. Su, and M.J. Lenardo. 2018. RELA haploinsufficiency in CD4 lymphoproliferative disease with autoimmune cytopenias. *J. Allergy Clin. Immunol.* 141:1507–1510.e1508. https://doi.org/10.1016/j.jaci.2017.11.036

Croxford, A.L., M. Lanzinger, F.J. Hartmann, B. Schreiner, F. Mair, P. Pelczar, B.E. Clausen, S. Jung, M. Greter, and B. Becher. 2015. The cytokine GM-CSF drives the inflammatory signature of CCR2+ monocytes and licenses autoimmunity. *Immunity*. 43:502–514. https://doi.org/10.1016/j.immuni.2015.08.010

de Oliveira, K.A., E. Kaergel, M. Heinig, J.F. Fontaine, G. Patone, E.M. Muro, S. Mathas, M. Hummel, M.A. Andrade-Navarro, N. Hübner, and C. Scheidereit. 2016. A roadmap of constitutive NF-κB activity in Hodgkin lymphoma: Dominant roles of p50 and p52 revealed by genome-wide analyses. *Genome Med.* 8:28. https://doi.org/10.1186/s13073-016-0280-5

Evaristo, C., S. Spranger, S.E. Barnes, M.L. Miller, L.L. Molinero, F.L. Locke, T.F. Gajewski, and M.-L. Alegre. 2016. Cutting edge: Engineering active IKKβ in T cells drives tumor rejection. *J. Immunol.* 196:2933–2938. https://doi.org/10.4049/jimmunol.1501144

Gerondakis, S., T.S. Fulford, N.L. Messina, and R.J. Grumont. 2014. NF-κB control of T cell development. *Nat. Immunol.* 15:15–25. https://doi.org/10.1038/ni.2785

Gerondakis, S., A. Strasser, D. Metcalf, G. Grigoriadis, J.Y. Scheerlinck, and R.J. Grumont. 1996. Rel-deficient T cells exhibit defects in production of interleukin 3 and granulocyte-macrophage colony-stimulating factor. *Proc. Natl. Acad. Sci. USA*. 93:3405–3409. https://doi.org/10.1073/pnas.93.8.3405

Gilmore, T.D., and M. Herscovitch. 2006. Inhibitors of NF-kappaB signaling: 785 and counting. *Oncogene*. 25:6887–6899. https://doi.org/10.1038/sj.onc.1209982

Giordano, M., R. Roncagalli, P. Bourdely, L. Chasson, M. Buferne, S. Yamasaki, R. Beyaert, G. van Loo, N. Auphan-Anezin, A.-M. Schmitt-Verhulst, and G. Verdeil. 2014. The tumor necrosis factor alpha-induced protein 3 (TNFAIP3, A20) imposes a brake on antitumor activity of CD8 T cells. *Proc. Natl. Acad. Sci. USA*. 111:11115–11120. https://doi.org/10.1073/pnas.1406259111

Grasso, C.S., J. Tsoi, M. Onyshchenko, G. Abril-Rodriguez, P. Ross-Macdonald, M. Wind-Rotolo, A. Champhekar, E. Medina, D.Y. Torrejon, D.S. Shin, et al. 2021. Conserved interferon-γ signaling drives clinical response to immune checkpoint blockade therapy in melanoma. *Cancer Cell*. 39:122. https://doi.org/10.1016/j.ccell.2020.11.015

Greve, B., R. Weissert, N. Hamdi, E. Bettelli, R.A. Sobel, A. Coyle, V.K. Kuchroo, K. Rajewsky, and M. Schmidt-Supprian. 2007. I kappa B kinase 2/beta deficiency controls expansion of autoreactive T cells and suppresses experimental autoimmune encephalomyelitis. *J. Immunol.* 179:179–185. https://doi.org/10.4049/jimmunol.179.1.179

Grinberg-Bleyer, Y., R. Caron, J.J. Seeley, N.S. De Silva, C.W. Schindler, M.S. Hayden, U. Klein, and S. Ghosh. 2018. The alternative NF-κB pathway in regulatory T cell homeostasis and suppressive function. *J. Immunol.* 200:2362–2371. https://doi.org/10.4049/jimmunol.1800042

Grinberg-Bleyer, Y., H. Oh, A. Desrichard, D.M. Bhatt, R. Caron, T.A. Chan, R.M. Schmid, U. Klein, M.S. Hayden, and S. Ghosh. 2017. NF-κB c-Rel is crucial for the regulatory T cell immune checkpoint in cancer. *Cell*. 170:1096–1108.e13. https://doi.org/10.1016/j.cell.2017.08.004

Heise, N., N.S. De Silva, K. Silva, A. Carette, G. Simonetti, M. Pasparakis, and U. Klein. 2014. Germinal center B cell maintenance and differentiation are controlled by distinct NF-κB transcription factor subunits. *J. Exp. Med.* 211:2103–2118. https://doi.org/10.1084/jem.20132613

Henriksson, J., X. Chen, T. Gomes, U. Ullah, K.B. Meyer, R. Miragaia, G. Duddy, J. Pramanik, K. Yusa, R. Lahesmaa, and S.A. Teichmann. 2019. Genome-wide CRISPR screens in T helper cells reveal pervasive crosstalk between activation and differentiation. *Cell*. 176:882–896.e18. https://doi.org/10.1016/j.cell.2018.11.044

Hilliard, B.A., N. Mason, L. Xu, J. Sun, S.-E. Lamhamedi-Cherradi, H.-C. Liou, C. Hunter, and Y.H. Chen. 2002. Critical roles of c-Rel in autoimmune inflammation and helper T cell differentiation. *J. Clin. Invest.* 110:843–850. https://doi.org/10.1172/JCI0215254

Joulia, E., M.F. Michieletto, A. Agesta, C. Peillex, V. Girault, A.L. Le Dorze, R. Peroceschi, F. Bucciarelli, M. Szelechowski, A. Chaubet, et al. 2024. Eomes-dependent mitochondrial regulation promotes survival of pathogenic CD4+ T cells during inflammation. *J. Exp. Med.* 221:e20230449. https://doi.org/10.1084/jem.20230449

Kamphorst, A.O., A. Wieland, T. Nasti, S. Yang, R. Zhang, D.L. Barber, B.T. Konieczny, C.Z. Daugherty, L. Koenig, K. Yu, et al. 2017. Rescue of exhausted CD8 T cells by PD-1-targeted therapies is CD28-dependent. *Science*. 355:1423–1427. https://doi.org/10.1126/science.aaf0683

Lalle, G., R. Lautraite, A. Voisin, J. Twardowski, P. Stéphan, M. Perrin-Niquet, R. Igalouzene, S.M. Soudja, J.C. Marie, M. Vocanson, et al. 2021a. A T cell-intrinsic function for NF-κB RelB in experimental autoimmune encephalomyelitis. *Sci. Rep.* 11:19674. https://doi.org/10.1038/s41598-021-99134-x

Lalle, G., J. Twardowski, and Y. Grinberg-Bleyer. 2021b. NF-kappaB in cancer immunity: Friend or Foe? *Cells* 10:355. https://doi.org/10.3390/cells10020355

Legut, M., Z. Gajic, M. Guarino, Z. Daniloski, J.A. Rahman, X. Xue, C. Lu, L. Lu, E.P. Mimitou, S. Hao, et al. 2022. A genome-scale screen for synthetic drivers of T cell proliferation. *Nature*. 603:728–735. https://doi.org/10.1038/s41586-022-04494-7

Lévy, R., D. Langlais, V. Beziat, F. Rapaport, G. Rao, T. Lazarov, M. Bourgey, Y.J. Zhou, C. Briand, K. Moriya, et al. 2021. Inherited human c-Rel deficiency disrupts myeloid and lymphoid immunity to multiple infectious agents. *J. Clin. Invest.* 131:e150143. https://doi.org/10.1172/JCI150143

Li, T., X. Li, A. Zamani, W. Wang, C.N. Lee, M. Li, G. Luo, E. Eller, H. Sun, S. Ghosh, et al. 2020. c-Rel is a myeloid checkpoint for cancer immunotherapy. *Nat. Cancer*. 1:507–517. https://doi.org/10.1038/s43018-020-0061-3

Li, X., J. Liu, J.K. Park, T.A. Hamilton, P. Rayman, E. Klein, M. Edinger, R. Tubbs, R. Bukowski, and J. Finke. 1994. T cells from renal cell carcinoma patients exhibit an abnormal pattern of kappa B-specific DNA-binding activity: A preliminary report. *Cancer Res.* 54:5424–5429.

Liu, X., Y. Wang, H. Lu, J. Li, X. Yan, M. Xiao, J. Hao, A. Alekseev, H. Khong, T. Chen, et al. 2019. Genome-wide analysis identifies NR4A1 as a key mediator of T cell dysfunction. *Nature*. 567:525–529. https://doi.org/10.1038/s41586-019-0979-8

Mc Guire, C., M. Prinz, R. Beyaert, and G. van Loo. 2013. Nuclear factor kappa B (NF-κB) in multiple sclerosis pathology. *Trends Mol. Med.* 19:604–613. https://doi.org/10.1016/j.molmed.2013.08.001

McGuire, K.L., and M. Iacobelli. 1997. Involvement of Rel, Fos, and Jun proteins in binding activity to the IL-2 promoter CD28 response element/AP-1 sequence in human T cells. *J. Immunol.* 159:1319–1327. https://doi.org/10.4049/jimmunol.159.3.1319

Monsma, P.C., and A. Brown. 2012. FluoroMyelin™ Red is a bright, photostable and non-toxic fluorescent stain for live imaging of myelin. *J. Neurosci. Methods*. 209:344–350. https://doi.org/10.1016/j.jneumeth.2012.06.015

Moriya, K., T. Nakano, Y. Honda, M. Tsumura, M. Ogishi, M. Sonoda, M. Nishitani-Isa, T. Uchida, M. Hbibi, Y. Mizoguchi, et al. 2023. Human RELA dominant-negative mutations underlie type I interferonopathy with autoinflammation and autoimmunity. *J. Exp. Med.* 220:e20212276. https://doi.org/10.1084/jem.20212276

Oeckinghaus, A., M.S. Hayden, and S. Ghosh. 2011. Crosstalk in NF-kappaB signaling pathways. *Nat. Immunol.* 12:695–708. https://doi.org/10.1038/ni.2065

Oh, H., Y. Grinberg-Bleyer, W. Liao, D. Maloney, P. Wang, Z. Wu, J. Wang, D.M. Bhatt, N. Heise, R.M. Schmid, et al. 2017. An NF-κB transcription-factor-dependent lineage-specific transcriptional program promotes regulatory T cell identity and function. *Immunity*. 47:450–465.e5. https://doi.org/10.1016/j.immuni.2017.08.010

Pesu, M., L. Muul, Y. Kanno, and J.J. O'Shea. 2006. Proprotein convertase furin is preferentially expressed in T helper 1 cells and regulates

interferon gamma. *Blood*. 108:983–985. https://doi.org/10.1182/blood-2005-09-3824

Powolny-Budnicka, I., M. Riemann, S. Tänzer, R.M. Schmid, T. Hehlgans, and F. Weih. 2011. RelA and RelB transcription factors in distinct thymocyte populations control lymphotoxin-dependent interleukin-17 production in γδ T cells. *Immunity*. 34:364–374. https://doi.org/10.1016/j.immuni.2011.02.019

Raveney, B.J., S. Oki, H. Hohjoh, M. Nakamura, W. Sato, M. Murata, and T. Yamamura. 2015. Eomesodermin-expressing T-helper cells are essential for chronic neuroinflammation. *Nat. Commun.* 6:8437. https://doi.org/10.1038/ncomms9437

Raveney, B.J.E., W. Sato, D. Takewaki, C. Zhang, T. Kanazawa, Y. Lin, T. Okamoto, M. Araki, Y. Kimura, N. Sato, et al. 2021. Involvement of cytotoxic Eomes-expressing CD4(+) T cells in secondary progressive multiple sclerosis. *Proc. Natl. Acad. Sci. USA* 118:e2021818118. https://doi.org/10.1073/pnas.2021818118

Rincón, M., and R.A. Flavell. 1994. AP-1 transcriptional activity requires both T-cell receptor-mediated and co-stimulatory signals in primary T lymphocytes. *EMBO J.* 13:4370–4381. https://doi.org/10.1002/j.1460-2075.1994.tb06757.x

Ruan, Q., V. Kameswaran, Y. Zhang, S. Zheng, J. Sun, J. Wang, J. DeVirgiliis, H.-C. Liou, A.A. Beg, and Y.H. Chen. 2011. The Th17 immune response is controlled by the Rel-RORγ-RORγ T transcriptional axis. *J. Exp. Med.* 208:2321–2333. https://doi.org/10.1084/jem.20110462

Saligrama, N., F. Zhao, M.J. Sikora, W.S. Serratelli, R.A. Fernandes, D.M. Louis, W. Yao, X. Ji, J. Idoyaga, V.B. Mahajan, et al. 2019. Opposing T cell responses in experimental autoimmune encephalomyelitis. *Nature*. 572:481–487. https://doi.org/10.1038/s41586-019-1467-x

Sareneva, T., K. Cantell, L. Pyhälä, J. Pirhonen, and I. Julkunen. 1993. Effect of carbohydrates on the pharmacokinetics of human interferon-gamma. *J. Interferon Res.* 13:267–269. https://doi.org/10.1089/jir.1993.13.267

Satoh, J., T. Misawa, H. Tabunoki, and T. Yamamura. 2008. Molecular network analysis of T-cell transcriptome suggests aberrant regulation of gene expression by NF-kappaB as a biomarker for relapse of multiple sclerosis. *Dis. Markers*. 25:27–35. https://doi.org/10.1155/2008/824640

Schafflick, D., C.A. Xu, M. Hartlehnert, M. Cole, A. Schulte-Mecklenbeck, T. Lautwein, J. Wolbert, M. Heming, S.G. Meuth, T. Kuhlmann, et al. 2020. Integrated single cell analysis of blood and cerebrospinal fluid leukocytes in multiple sclerosis. *Nat. Commun.* 11:247. https://doi.org/10.1038/s41467-019-14118-w

Schmidt, R., Z. Steinhart, M. Layeghi, J.W. Freimer, R. Bueno, V.Q. Nguyen, F. Blaeschke, C.J. Ye, and A. Marson. 2022. CRISPR activation and interference screens decode stimulation responses in primary human T cells. *Science*. 375:eabj4008. https://doi.org/10.1126/science.abj4008

Schraml, B.U., K. Hildner, W. Ise, W.L. Lee, W.A. Smith, B. Solomon, G. Sahota, J. Sim, R. Mukasa, S. Cemerski, et al. 2009. The AP-1 transcription factor Batf controls T(H)17 differentiation. *Nature*. 460:405–409. https://doi.org/10.1038/nature08114

Seo, H., E. González-Avalos, W. Zhang, P. Ramchandani, C. Yang, C.J. Lio, A. Rao, and P.G. Hogan. 2021. BATF and IRF4 cooperate to counter exhaustion in tumor-infiltrating CAR T cells. *Nat. Immunol.* 22:983–995. https://doi.org/10.1038/s41590-021-00964-8

Shah, K., A. Al-Haidari, J. Sun, and J.U. Kazi. 2021. T cell receptor (TCR) signaling in health and disease. *Signal Transduct. Target. Ther.* 6:412. https://doi.org/10.1038/s41392-021-00823-w

Shifrut, E., J. Carnevale, V. Tobin, T.L. Roth, J.M. Woo, C.T. Bui, P.J. Li, M.E. Diolaiti, A. Ashworth, and A. Marson. 2018. Genome-wide CRISPR screens in primary human T cells reveal key regulators of immune function. *Cell*. 175:1958–1971.e15. https://doi.org/10.1016/j.cell.2018.10.024

Stamou, P., and D.L. Kontoyiannis. 2010. Posttranscriptional regulation of TNF mRNA: A paradigm of signal-dependent mRNA utilization and its relevance to pathology. *Curr. Dir. Autoimmun.* 11:61–79. https://doi.org/10.1159/000289197

Steinman, L. 2001. Myelin-specific CD8 T cells in the pathogenesis of experimental allergic encephalitis and multiple sclerosis. *J. Exp. Med.* 194:F27–F30. https://doi.org/10.1084/jem.194.5.F27

Su, B., E. Jacinto, M. Hibi, T. Kallunki, M. Karin, and Y. Ben-Neriah. 1994. JNK is involved in signal integration during costimulation of T lymphocytes. *Cell*. 77:727–736. https://doi.org/10.1016/0092-8674(94)90056-6

Visekruna, A., M. Huber, A. Hellhund, E. Bothur, K. Reinhard, N. Bollig, N. Schmidt, T. Joeris, M. Lohoff, and U. Steinhoff. 2010. c-Rel is crucial for the induction of Foxp3(+) regulatory CD4(+) T cells but not T(H)17 cells. *Eur. J. Immunol.* 40:671–676. https://doi.org/10.1002/eji.200940260

Visekruna, A., T. Linnerz, V. Martinic, N. Vachharajani, S. Hartmann, H. Harb, T. Joeris, P.I. Pfefferle, M.J. Hofer, and U. Steinhoff. 2015. Transcription factor c-Rel plays a crucial role in driving anti-CD40-mediated innate colitis. *Mucosal Immunol.* 8:307–315. https://doi.org/10.1038/mi.2014.68

Voisin, A., and Y. Grinberg-Bleyer. 2021. The many-sided contributions of NF-κB to T-cell biology in health and disease. *Int. Rev. Cell Mol. Biol.* 361:245–300. https://doi.org/10.1016/bs.ircmb.2020.10.006

Webb, L.V., A. Barbarulo, J. Huysentruyt, T. Vanden Berghe, N. Takahashi, S. Ley, P. Vandenabeele, and B. Seddon. 2019. Survival of single positive thymocytes depends upon developmental control of RIPK1 kinase signaling by the IKK complex independent of NF-κB. *Immunity*. 50:348–361.e4. https://doi.org/10.1016/j.immuni.2019.01.004

Weih, F., D. Carrasco, S.K. Durham, D.S. Barton, C.A. Rizzo, R.P. Ryseck, S.A. Lira, and R. Bravo. 1995. Multiorgan inflammation and hematopoietic abnormalities in mice with a targeted disruption of RelB, a member of the NF-kappa B/Rel family. *Cell*. 80:331–340. https://doi.org/10.1016/0092-8674(95)90416-6

Wong, D., A. Teixeira, S. Oikonomopoulos, P. Humburg, I.N. Lone, D. Saliba, T. Siggers, M. Bulyk, D. Angelov, S. Dimitrov, et al. 2011. Extensive characterization of NF-κB binding uncovers non-canonical motifs and advances the interpretation of genetic functional traits. *Genome Biol.* 12:R70. https://doi.org/10.1186/gb-2011-12-7-r70

Yamazaki, S., Y. Tanaka, H. Araki, A. Kohda, F. Sanematsu, T. Arasaki, X. Duan, F. Miura, T. Katagiri, R. Shindo, et al. 2017. The AP-1 transcription factor JunB is required for Th17 cell differentiation. *Sci. Rep.* 7:17402. https://doi.org/10.1038/s41598-017-17597-3

Yan, H., X. Duan, H. Pan, N. Holguin, M.F. Rai, A. Akk, L.E. Springer, S.A. Wickline, L.J. Sandell, and C.T. Pham. 2016. Suppression of NF-κB activity via nanoparticle-based siRNA delivery alters early cartilage responses to injury. *Proc. Natl. Acad. Sci. USA*. 113:E6199–E6208. https://doi.org/10.1073/pnas.1608245113

Yan, J., C.M. Winterford, V.S. Catts, B.K. Pat, M.P. Pender, P.A. McCombe, and J.M. Greer. 2018. Increased constitutive activation of NF-κB p65 (RelA) in peripheral blood cells of patients with progressive multiple sclerosis. *J. Neuroimmunol.* 320:111–116. https://doi.org/10.1016/j.jneuroim.2018.04.002

Zhang, H., J. Bi, H. Yi, T. Fan, Q. Ruan, L. Cai, Y.H. Chen, and X. Wan. 2017. Silencing c-Rel in macrophages dampens Th1 and Th17 immune responses and alleviates experimental autoimmune encephalomyelitis in mice. *Immunol. Cell Biol.* 95:593–600. https://doi.org/10.1038/icb.2017.11

Zhao, B., L.A. Barrera, I. Ersing, B. Willox, S.C. Schmidt, H. Greenfeld, H. Zhou, S.B. Mollo, T.T. Shi, K. Takasaki, et al. 2014. The NF-κB genomic landscape in lymphoblastoid B cells. *Cell Rep.* 8:1595–1606. https://doi.org/10.1016/j.celrep.2014.07.037

Zhao, M., P. Chauhan, C.A. Sherman, A. Singh, M. Kaileh, K. Mazan-Mamczarz, H. Ji, J. Joy, S. Nandi, S. De, et al. 2023. NF-κB subunits direct kinetically distinct transcriptional cascades in antigen receptor-activated B cells. *Nat. Immunol.* 24:1552–1564. https://doi.org/10.1038/s41590-023-01561-7

Zhu, J., and W.E. Paul. 2010. Heterogeneity and plasticity of T helper cells. *Cell Res.* 20:4–12. https://doi.org/10.1038/cr.2009.138

Supplemental material

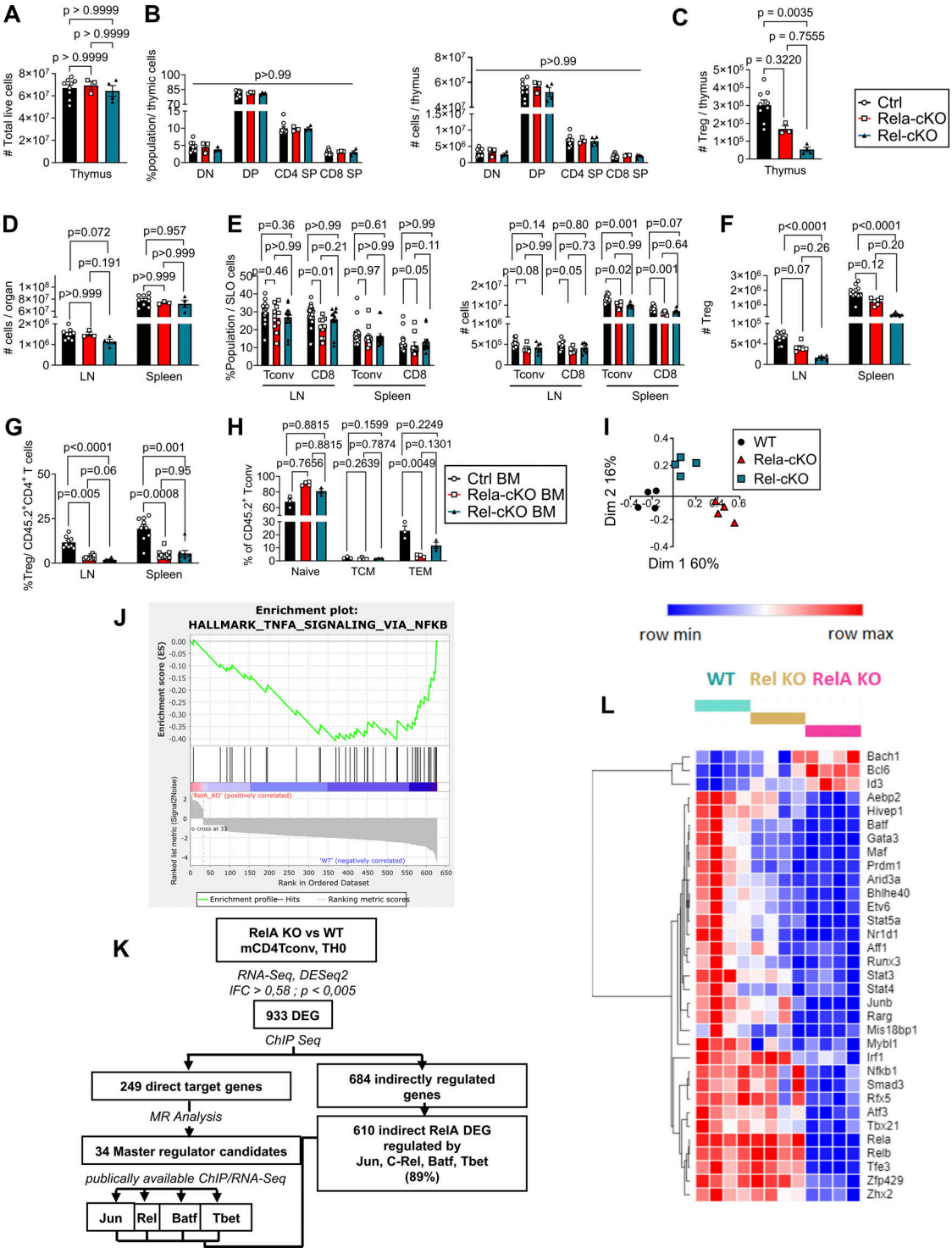

Figure S1. **The role of RelA and c-Rel in Tconv at steady-state. (A–F)** Thymus, spleen, and peripheral LN from control (CD4^{cre}), *Rela*-cKO, and *Rel*-cKO mice were analyzed by flow cytometry (mean ± SEM of 3–9 mice/group from two experiments). **(A–C)** Analysis of the thymus. **(A)** Number of total live cells. **(B)** Proportions and absolute numbers of double negative (DN), double positive (DP), and simple positive (SP) CD4$^+$ and CD8$^+$ T cells. **(C)** Quantification of live Tregs. **(D–H)** Analysis of spleens and peripheral LNs. **(D)** Number of total live cells. **(E)** Proportions and absolute numbers of Tconv and CD8$^+$ T cells among total live cells. **(F)** Quantification of live Tregs. **(G and H)** Analysis of mixed BM chimeras as in Fig. 1, by flow cytometry (mean ± SEM of *n* = 10 mice/group from two experiments). **(G)** Proportion of FoxP3$^+$ Treg among CD45.2$^+$ CD4$^+$ cells in secondary lymphoid organs. **(H)** Proportion of naive (CD44$^-$CD62L$^+$) TCM (T central memory) (CD44$^+$CD62L$^+$) and TEM (CD44$^+$CD62L$^-$) among CD45.2$^+$ Tconv in spleen. **(I–L)** Analysis of RNA-seq data from Fig. 1 (*n* = 4 independent samples/genotype [2 mice/sample] from two experiments sequenced simultaneously). **(I)** Correspondence analysis of mRNA counts of all the genes of WT (blue points), *Rel*-cKO (orange squares), and *RelA*-KO (pink triangles) murine CD4$^+$ Tconv before differential expression analysis. **(J)** GSEA plot from Rela-cKO dataset showing decreased expression of known NF-κB–dependent genes. **(K)** Strategy for the identification of indirect transcriptional regulators. **(L)** Expression of the 34 master regulator candidates. lFC, log2 fold change; MR analysis, master regulator analysis.

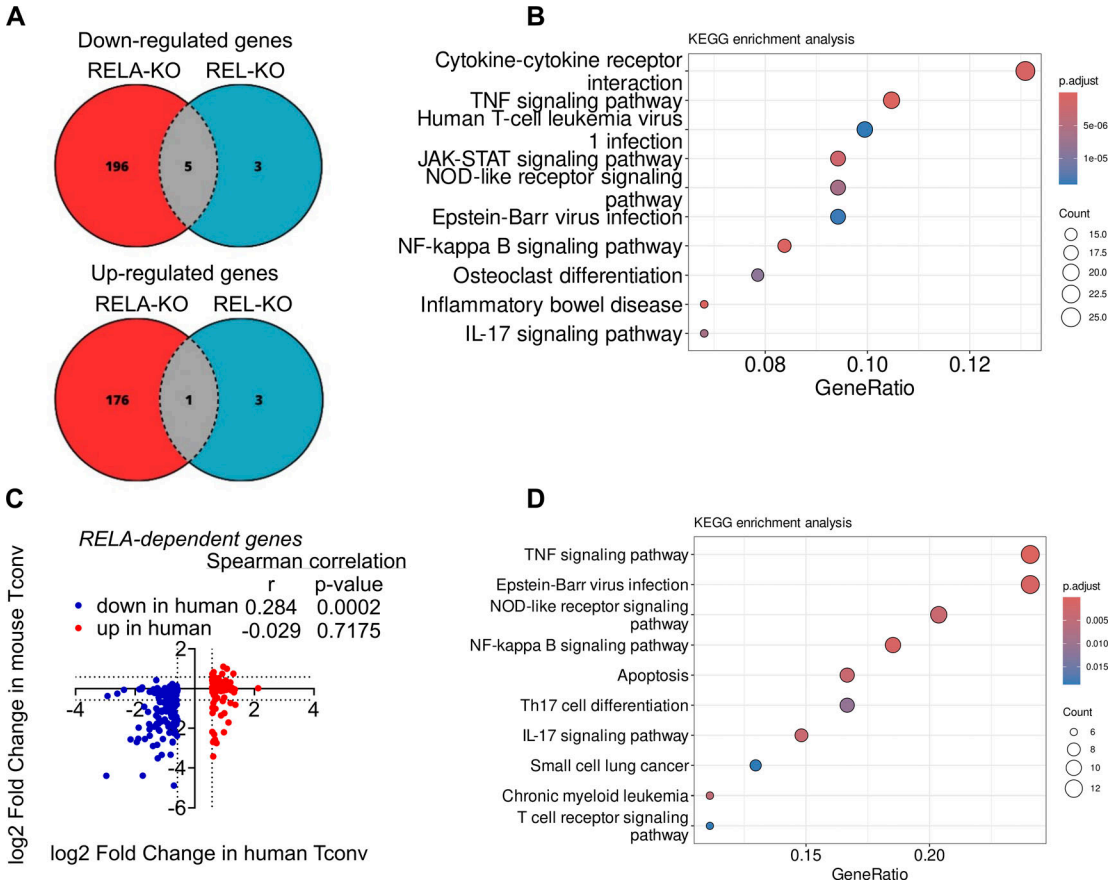

Figure S2. **RNA-seq analysis of human gene-edited Tconv.** *n* = 4 experiments with independent donors, sequenced simultaneously. **(A)** Venn partition diagram showing the overlap between RelA and c-Rel–regulated DEGs. (log_2 fold change >0.58, P < 0.005). **(B)** KEGG enrichment analysis of *RELA*-KO DEGs. **(C)** Expression of the 378 human *RELA*-KO DEGs in the mouse dataset. **(D)** KEGG enrichment analysis of the 80 common downregulated genes in mouse and human *RELA*-KO Tconv.

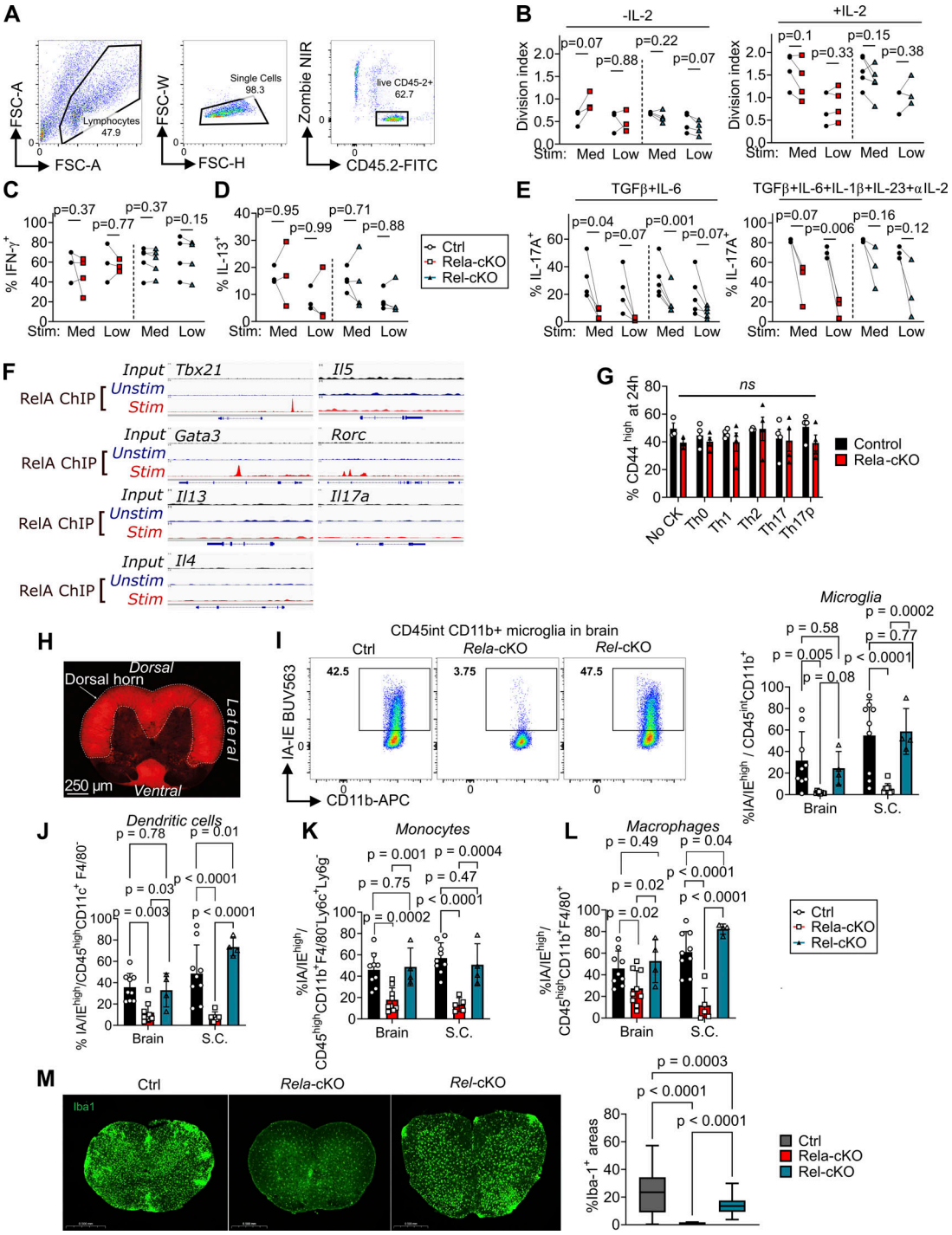

Figure S3. **RelA and c-Rel in TH differentiation and pathogenicity in EAE. (A–E)** Naive Tconv from control ($CD4^{cre}$), *Rela*-cKO, and *Rel*-cKO mice were isolated, stimulated with medium or low concentrations of soluble anti-CD3 and feeders, and cultured with or without IL-2 (B), or under Th1 (C), Th2 (D), or Th17 (E) for 4 days as detailed in Materials and methods, and their phenotype was analyzed by FACS after PMA-ionomycin restimulation. **(A)** Gating strategy for Tconv analysis. **(B–E)** Cumulative data from at least three experiments are shown. Each line represents an independent experiment; multiple paired t-tests were used. **(F)** Data from RelA ChIP-Seq in Tconv, from Oh et al. (2017), were visualized using Integrative Genome Viewer. **(G)** Naive Tconv were isolated and cultured as above for 24 h. The proportion of $CD44^{hi}$ cells was assessed by FACS. Mean ± SEM from three to four experiments are shown; each dot represents an individual experiment. Multiple Mann–Whitney tests were used; ns = non-significant. **(H–M)** EAE was induced in control ($CD4^{cre}$), *Rela*-cKO, and *Rel*-cKO mice. **(H)** Representative Fluoromyelin staining in the spinal cord, showing delimitation of the dorsal horn, used for statistical quantification in Fig. 4. **(I–L)** At D21, MHC-II expression was measured by FACS in myeloid cells (mean ± SEM of *n* = 4–9 mice/group from two experiments). (I) $CD45^{int}CD11b^{+}$ microglia cells, (J) $CD45^{high}TCR\beta^{-}CD11c^{+}F4/80^{-}$ dendritic cells, (K) $CD45^{high}TCR\beta^{-}CD11b^{+}F4/80^{-}Ly6C^{+}Ly6G^{-}$ monocytes, and (L) $CD45^{high}TCR\beta^{-}CD11b^{+}F4/80^{+}$ macrophages. Mean ± SEM are shown; each dot represents an individual mouse from two independent experiments. **(M)** Sections of spinal cords at D15, stained for Iba-1. Representative images (left) and cumulative proportion of Iba-1^{+} areas of 35 to 59 cross-sections from four to five mice/group of two independent experiments (right) are shown as box and whiskers plot (min to max). Kruskal–Wallis (I–L) and one-way ANOVA test (M) were used.

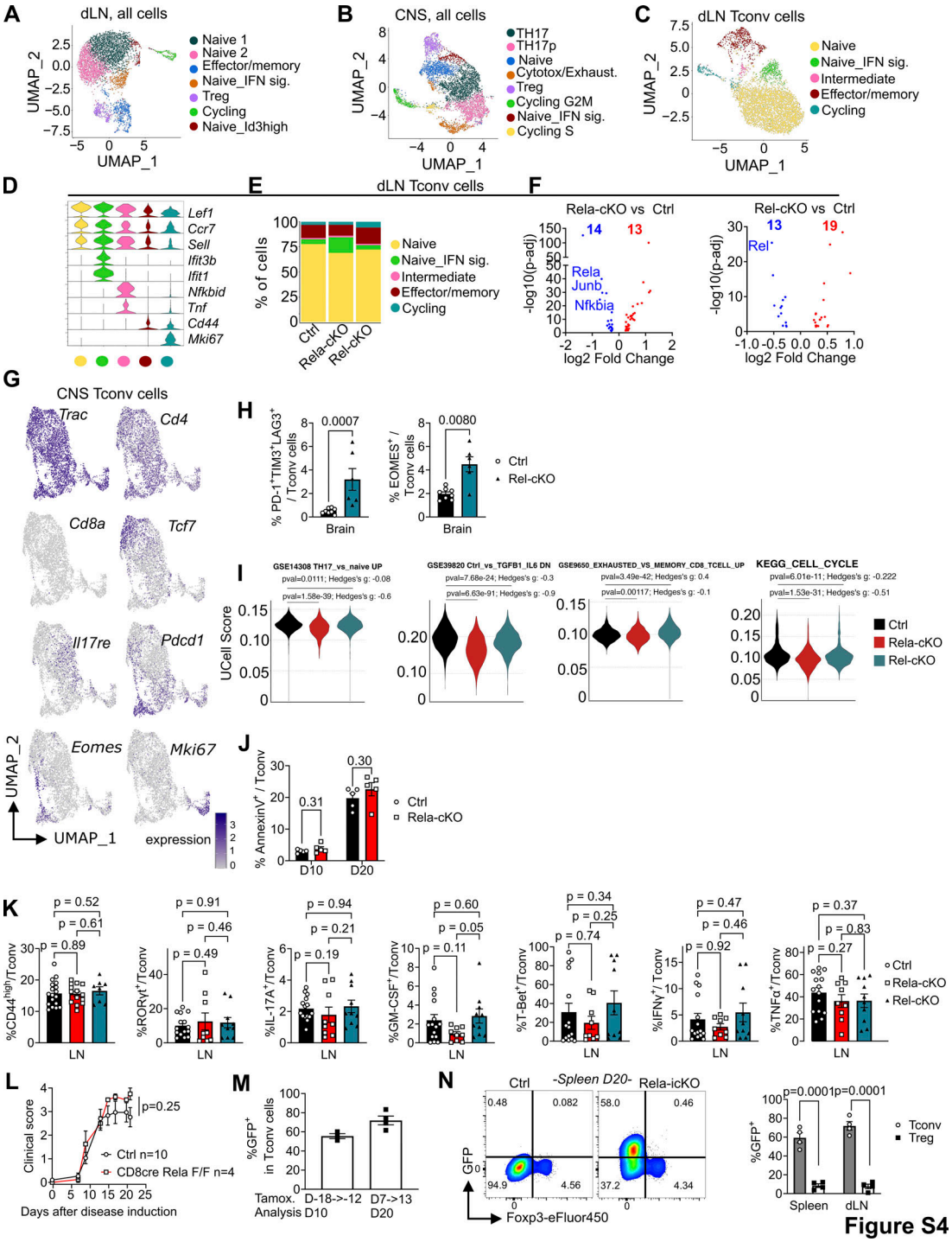

Figure S4. **The role of RelA and c-Rel in Tconv during EAE.** EAE was induced in control (CD4^{cre}), *Rela*-cKO, and *Rel*-cKO mice. **(A–G)** dLN and CNS-sorted CD4$^+$ T cells were analyzed by scRNA-seq as in Fig. 5 (performed once with five to six pooled mice/genotype). **(A)** UMAP projection of total CD4$^+$ T cells in each dLN. **(B)** UMAP projection of total CD4$^+$ T cells in each dLN. **(C)** UMAP projection and Seurat clustering of dLN-Tconv upon removal of Treg cells. **(D)** Violin plot showing expression of selected cluster-defining markers in dLN. **(E)** Distribution of the eight clusters in each genotype in dLN. **(F)** Volcano plot representation of DEGs in dLN (blue: downregulated, red: upregulated, p-adj cutoff <0.05). **(G)** Expression of selected markers projected on UMAP. **(H)** FACS analysis of the proportion of exhausted (left) and EOMES$^+$ cytotoxic (right) Tconv cells in the brain at D20 (mean ± SEM of *n* = 6–8 mice/group from two experiments). **(I)** Enrichment of the indicated signatures in CNS-infiltrating Tconv scRNA-seq data. **(J)** Proportion of apoptotic Annexin V$^+$ Tconv cells in the brain at D10 and D20 (mean ± SEM of two experiments; each dot represents a mouse). **(K)** dLN Tconv were analyzed by FACS 20 days after disease induction, after PMA-ionomycin restimulation (mean ± SEM of 8–15 mice/group from three independent experiments). **(L)** EAE was induced in control and CD8^{cre}Rela$^{F/F}$ mice; clinical scores are shown as mean ± SEM of one experiment with 4–10 mice/group. **(M and N)** Tamoxifen was administered to control (CD4$^{cre\text{-}ert2}$) and *Rela*-icKO mice as in Fig. 6 C. **(M)** Mean ± SEM of GFP$^+$ in Tconv cells at the indicated time points (*n* = 3–4/time point, two experiments). **(N)** Mean ± SEM of GFP$^+$ cells in Tconv and Treg cells at D20 following tamoxifen administration from D7 to D13 points (*n* = 4 mice, two experiments). Mann–Whitney (H, J, and N) Wilcoxon and Hedge's G (I), Kruskal–Wallis (K), and two-way ANOVA followed by Bonferroni's post-test (L) analyses were used.

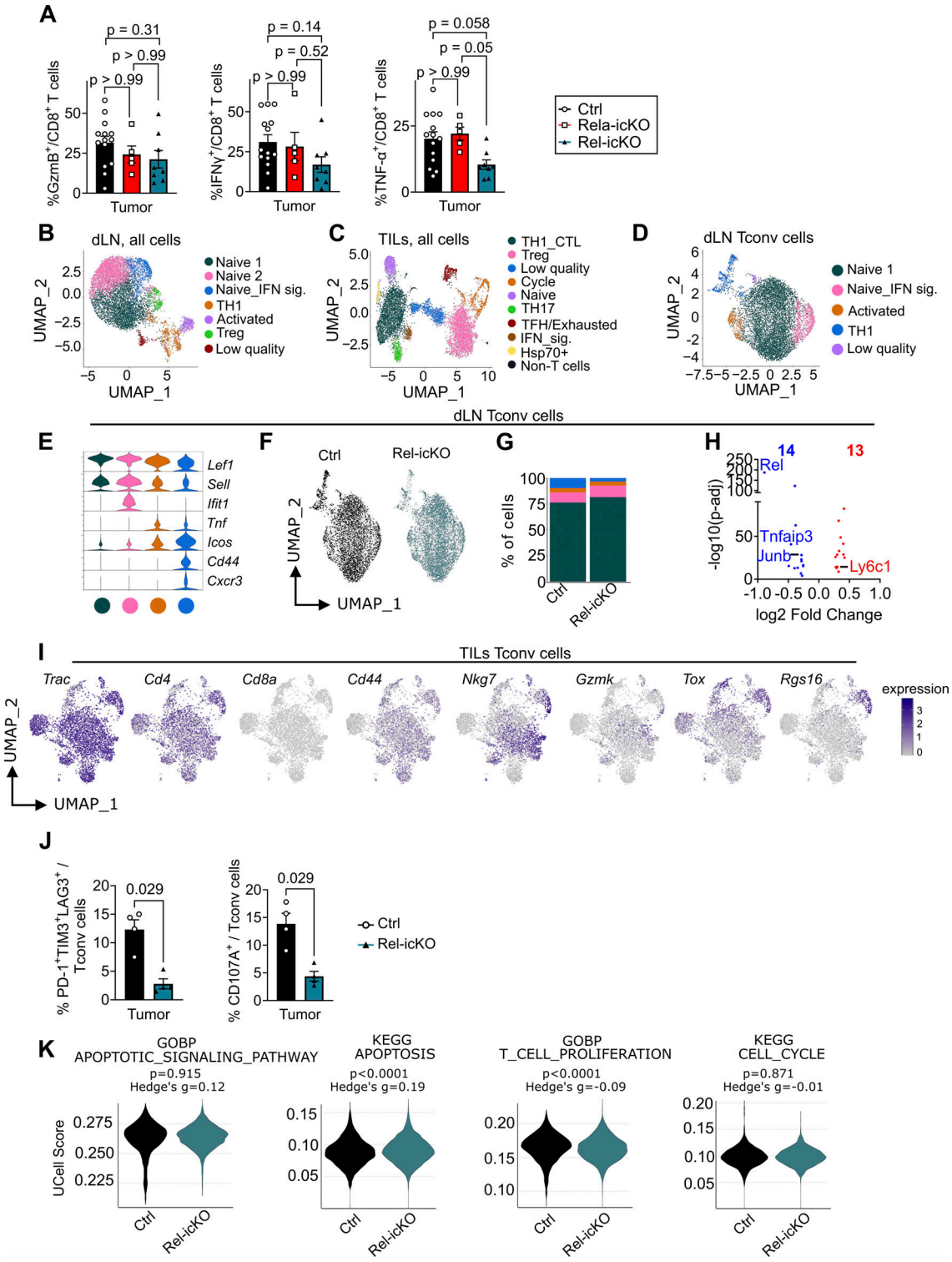

Figure S5. **The role of c-Rel in Tconv during tumor immunity.** Control (CD4$^{cre\text{-}ert2}$), *Rela*-icKO, and *Rel*-icKO mice were treated with tamoxifen from D1 to D7 and transplanted with B16-OVA melanoma cells as in Fig. 6. **(A)** FACS analysis of tumor-infiltrating CD8$^+$ T cells as D19 following PMA-ionomycin stimulation. Data are shown as mean ± SEM of 5–14 mice/group from two experiments; Kruskal–Wallis tests were used. **(B–J)** scRNA-seq analysis of dLN and tumor CD4$^+$ T cells (performed once with six to seven pooled mice/genotype). **(B and C)** UMAP projection of total CD4$^+$ T cells in each tissue. **(D)** UMAP projection and Seurat clustering of dLN Tconv upon removal of Treg cells. **(E)** Violin plots showing expression of selected cluster-defining markers in dLN. **(F)** Global distribution of Ctrl and *Rel*-deficient dLN Tconv on UMAP. **(G)** Distribution of the four clusters in each genotype in dLN. **(H)** Volcano plot representation of DEGs in dLN (blue: downregulated, red: upregulated, p-adj cutoff <0.05). **(I)** Expression of selected markers projected on UMAP. **(J)** FACS analysis of the proportion of exhausted (left) and CD107A$^+$ cytotoxic (right) Tconv cells in tumors at D19 (mean ± SEM of four mice/group from two experiments). **(K)** Expression of different GSEA signatures related to apoptosis and proliferation in tumor-infiltrating Tconv scRNA-seq dataset. Kruskal–Wallis tests (A), Wilcoxon and Hedge's G (J), and Mann–Whitney (K) tests were used. GOBP, Gene Ontology Biological Process.

Provided online is Table S1, which lists FACS and western blot antibodies used in this study.